CUKUROVA UNIVERSITY

INSTITUTE OF NATURAL AND APPLIED SCIENCES

MSc THESIS

Design and Simulation of a High Sensitive Graphene based ISFET pH Sensor with Readout Circuit

Ahmed W M HARB

Department of Biomedical Engineering

August, 2023

CUKUROVA UNIVERSITY

INSTITUTE OF NATURAL AND APPLIED SCIENCES

MSc THESIS APPROVAL

Design and Simulation of a High Sensitive Graphene based ISFET pH Sensor with Readout Circuit

---

Ahmed W M HARB

Department of Biomedical Engineering

This Master's Thesis was evaluated by the following Jury Members on 24/08/2023 and was approved by unanimity / majority of votes.

Jury : Assist. Prof. Dr. Mustafa İSTANBULLU (Advisor) ……

: Prof. Dr. Mutlu AVCI ……

: Assoc. Prof. Dr. Mahmud Yusuf TANRIKULU ……

This Thesis was written in the Department of Biomedical Engineering, Institute of Natural and Applied Sciences.

Thesis Number:

Prof. Dr. Sadık DİNÇER
Director
Institute of Natural and Applied Sciences

This work was supported by the Scientific Research Project Unit of Çukurova University.
Project ID: FYL-2022-15581

CONTENTS

ABSTRACT I
ÖZ II
ACKNOWLEDGEMENTS VI
LIST OF TABLES VII
LIST OF FIGURES VIII
SYMBOLS AND ABBREVIATIONS IX
1. INTRODUCTION 1
2. PRELIMINARY WORK 5
2.1. Introduction 5
2.2. pH Sensing Technologies 5
2.3. Ion-Sensitive Field-Effect Transistors (ISFETs) 6
2.4. Graphene-Based Dual-Gate ISFETs 7
2.5. Challenges and Future Directions 7
2.6. Conclusion 7
3. ISFET BIOSENSORS 9
3.1. Introduction and history of ISFET 9
3.2. ISFET working principle 9
3.3. ISFET and MOSFET: Basic Analogy 10
3.4. Electrochemistry of Ionic Solutions (Electrolytes) 11
3.5. Concept of pH (Power of Hydrogen) 12
3.6. pH Sensing Insulators 13
3.7. Reference electrode 14
3.8. Gate structures 15
3.9. Biosensing applications 16
4. GRAPHENE 19
4.1. Properties of Graphene: Electronic, Mechanical and Chemical 19
4.2. Graphene-Based Biosensors 20
4.3. Challenges and Future Perspectives 21
5. MICROFABRICATION PROCESS 23
5.1. Basics of microfabrication 23
5.2. Diffusion 25
5.3. Ion Implantation 26
5.4. Lithography 28
5.5. Etching 29
5.6. Metallization Process 31

6. DESIGN OF GRAPHENE-BASED NANOSTRUCTURED ISFET BIOSENSOR 33
6.1. Structure and Method of the proposed ISFET 33
6.2. Microfabrication of the proposed ISFET 36
6.3. Extracting parameters of the proposed ISFET 39
6.4. Simulation Results 40
6.4.1. Electrical Characteristics 40
6.4.2. Sensitivity Analysis 41
7. READOUT CIRCUIT: DESIGN, MODELLING AND ANALYSIS 43
7.1. Cadence Virtuoso: Overview 43
7.2. Design and development of ISFET and electrolyte models 43
7.2.1. Graphene ISFET model 43
7.2.2. Electrolyte model 44
7.3. Readout circuit: MOSFET differential amplifier 47
7.4. Simulation Results 50
7.4.1. Sensitivity Analysis 50
7.4.2. Linearity test 51
7.4.3. Stability analysis 51
7.4.4. Temperature-dependency test 52
8. CONCLUSIONS 53
REFERENCES 55
CURRICULUM VITAE 59
APPENDICES 60

CUKUROVA UNIVERSITY
INSTITUTE OF NATURAL AND APPLIED SCIENCES

MSc THESIS

Design and Simulation of a High Sensitive Graphene based ISFET pH Sensor with Readout Circuit

Ahmed W M HARB

Advisor: Assist. Prof. Dr. Mustafa ISTANBULLU

Department of Biomedical Engineering

ABSTRACT

Electrochemical sensors are devices that use electrochemical reactions to detect and measure the concentration of analytes in a sample. As an electrochemical sensor, an ion-sensitive field-effect transistor, ISFET, is the basic structure of a biosensor. This thesis presents a high-sensitive pH sensor with a graphene-based dual-gate ISFET. Design and simulations of the proposed device are performed on SILVACO TCAD (Technology Computer Aided Design) software and Cadence Virtuoso environment. Graphene and aluminum oxide are used as channel and sensing film, respectively. The channel thickness is 10 nm, while the thickness of the device is 800 nm. The transfer and output characteristic curves of the device are obtained through simulations. Furthermore, Linearity, Stability and Temperature-dependency of the proposed device have been analyzed and discussed after designing a readout circuit using the 90nm Generic Process Design Kit (gpdk090) library. The effects of the back gate, channel material, and sensitive layer on device performance are evaluated by assessing the electrical characteristics, threshold voltage, and drain current. The sensitivity of the proposed device is achieved, approximately 18 times the Nernst limit, as 1066 mV/pH, which is the best performance score in the literature. The proposed device offers a novel ISFET structure with reliable and higher detection sensitivity.

Keywords: ISFET, Biosensor, graphene, sensitivity, Cadence.

ÇUKUROVA ÜNİVERSİTESİ
FEN BİLİMLERİ ENSTİTÜSÜ

YÜKSEK LİSANS TEZİ

Okuma Devreli Yüksek Hassasiyetli Grafen Tabanlı ISFET pH Sensörünün Tasarımı ve Simülasyonu

Ahmed W M HARB

Danışman: Dr. Mustafa ISTANBULLU

Biyomedikal mühendisliği Anabilim Dalı

ÖZ

Elektrokimyasal sensörler, bir numunedeki analitlerin konsantrasyonunu tespit etmek ve ölçmek için elektrokimyasal reaksiyonları kullanan cihazlardır. Bir elektrokimyasal sensör olarak, iyona duyarlı alan etkili bir transistör olan ISFET, bir biyosensörün temel yapısıdır. Bu tez, grafen tabanlı çift kapılı ISFET'e sahip yüksek hassasiyetli bir pH sensörü sunar. Önerilen cihazın tasarımı ve simülasyonları SILVACO TCAD (Technology Computer Aided Design) yazılımı ve Cadence Virtuoso ortamında gerçekleştirilmiştir. Grafen ve alüminyum oksit sırasıyla kanal ve algılama filmi olarak kullanılır. Kanal kalınlığı 10 nm iken cihazın kalınlığı 800 nm'dir. Simülasyonlar yoluyla cihazın transfer ve çıkış karakteristik eğrileri elde edilmiştir. Ayrıca, 90nm Generic Process Design Kit (gpdk090) kitaplığı kullanılarak bir okuma devresi tasarlandıktan sonra, önerilen cihazın Lineerliği, Kararlılığı ve Sıcaklığa bağlılığı analiz edilmiş ve tartışılmıştır. Arka kapı, kanal malzemesi ve hassas katmanın cihaz performansı üzerindeki etkileri, elektriksel özellikler, eşik voltajı ve drenaj akımı değerlendirilerek değerlendirilir. Önerilen cihazın hassasiyeti literatürdeki en iyi performans skoru olan 1066 mv/pH olarak Nernst sınırının yaklaşık 18 katı olarak elde edilmiştir. Önerilen cihaz, güvenilir ve daha yüksek algılama hassasiyetine sahip yeni bir ISFET yapısı sunmaktadır.

Anahtar Kelimeler: ISFET, sensör, Grafen, duyarlılık, Cadence.

GENİŞLETİLMİŞ ÖZET

Sağlık hizmetlerinden çevresel izlemeye kadar çeşitli alanlarda biyosensörler, biyomoleküllerin hassas ve seçici tespiti için gerekli araçlar haline gelmiştir. Grafen bazlı yeni bir çift kapılı nanoyapılı İyon Hassas Alan Etkili Transistör (ISFET) biyosensörün tasarımı ve simülasyonu bu tezde ayrıntılı olarak incelenmiştir. Biyosensörün amacı, geleneksel ISFET cihazlarının sınırlamalarının üstesinden gelmek ve grafenin istisnai özelliklerini kullanarak ve bir sofistike çift kapılı mimari.

Grafen bazlı çift kapılı ISFET biyosensörün tasarımı ve simülasyonu bu tezde ayrıntılı olarak incelenmiştir. Ana amaç, grafenin istisnai özelliklerinden yararlanmak ve geleneksel ISFET biyosensörlerinin sınırlamalarının üstesinden gelmek için sofistike bir çift kapı mimarisine dahil etmekti. Sekiz bölüm araştırma yolculuğunu oluşturdu ve her biri biyosensör teknolojisinin ilerlemesine yardımcı olan değerli bilgiler sağladı.

Bu tezin temel bölümleri ISFET biyosensörlerinin kapsamlı bir şekilde anlaşılmasını sağlamıştır. Bu cihazlar, hassasiyetleri, seçiciliği ve çeşitli alanlardaki potansiyel uygulamaları nedeniyle büyük umut vaat ediyor. Biyolojik etkileşimler ve elektronik tepkiler arasındaki karmaşık ilişki, ISFET'lerin moleküler ve elektronik dünyalar arasındaki boşluğu doldurmadaki kritik rolünün altını çizerek çözülmüştür.

Tezin bağlamı, biyosensörlerin değerini ve bunların bilim ve tıbbın ilerlemesine katkısını vurgulayan giriş ile belirlenmiştir. Grafen bazlı çift kapılı nanoyapılı ISFET biyosensörün tasarımı ve simülasyonu araştırmanın ana hedefidir. Girişte, biyosensörlerin önemini ve grafeni bir algılama malzemesi olarak keşfetmenin arkasındaki motivasyonu vurgulamak sağlanır. Sonraki bölümler için yön belirleyen özel hedefler ana hatlarıyla belirtilmiştir. Bölüm, araştırma yapısına genel bir bakış sunmakta ve ayrıca aşağıdaki bölümlerin nasıl düzenleneceğini açıklamaktadır.

Bölüm 2, ISFET biyosensörleri ve grafen üzerindeki önceki çalışmaları gözden geçirerek ilgili çalışmaları tanımlamak ve belirli hedefleri formüle etmek için genel bir bakış sunmaktadır. ISFET biyosensörlerinin operasyonel ilkeleri ve uygulamaları, sınırlamalar ve yaratıcı çözümlere duyulan ihtiyaç vurgulanarak bu kapsamlı literatür incelemesinde ayrıntılı olarak incelenmiştir. İnceleme, pH algılamasında bu teknolojinin ilerlemeleri, zorlukları ve potansiyel uygulamaları hakkında kapsamlı bir anlayış sağlamayı amaçlamaktadır

Tezin kalbi olan Bölüm 3 ila 5, temel konuların derinliklerine iner. Bölüm 3, ISFET Biosensors dünyasını ortaya çıkarır ve biyosensing alanındaki önemli rollerini çözer. Bölüm, ISFET'lerin tarihsel gelişimini, operasyonel ilkelerini ve çeşitli konfigürasyonlarını geçerek hassasiyetlerini, seçiciliklerini ve gerçek dünya uygulamalarını vurgulamaktadır.

ISFET biyosensörlerinin çalışmaları ve kullanımları Bölüm 3'te ayrıntılı olarak incelenmiştir. Hassasiyetini ve seçiciliğini artıracak stratejiler geliştirmek için ISFET'in iyon konsantrasyonundaki değişikliklere tepkisinin altında yatan mekanizmaları anlamak önemlidir. Bu

bölüm ISFET'in tarihi ve çalışma prensibi gibi bazı alt bölümleri araştırmaktadır. Ayrıca, MOSFET ve ISFET arasındaki temel benzetmeyi tartışır. Bundan sonra, elektrolitler, pH kavramı, algılama İzolatörleri, referans elektrot, kapı yapısı ve biyo-duyarlı uygulamalar sırasıyla açıklanmaktadır.

Grafen, dikkat çekici özelliklerini vurgulayarak Bölüm 4'teki biyo-duyarlı uygulamalar için ideal bir malzeme olarak konumlandırılmıştır. Grafen geniş bir yüzey alanına, olağanüstü elektrik iletkenliğine ve biyouyumluluğa sahiptir. Bu bölüm, grafenin biyosensing uygulamaları için mükemmel bir malzeme olmasını sağlayan benzersiz özelliklerini araştırmaktadır. Grafinin özel elektronik, mekanik ve kimyasal özelliklerini araştırır ve ISFET biyosensör performansını nasıl artırabileceğini gösterir. Olağanüstü nitelikleri ve geniş uygulama yelpazesi nedeniyle son zamanlarda çok dikkat çekti. Bu bölüm, grafenin biyosensing uygulamaları için mükemmel bir malzeme olmasını sağlayan olağanüstü özelliklerini araştırmaktadır. Grafinin özel elektronik, mekanik ve kimyasal özelliklerini inceler ve ISFET biyosensör performansını nasıl artırabileceğini gösterir. Bölüm ayrıca, önerilen ISFET biyosensöründe bir kanal malzemesi olarak kullanılacak grafeni sentezlemek ve işlevselleştirmek için çeşitli yöntemleri tartışmaktadır.

Mikrofabrikasyon süreci Bölüm 5'te tartışılmaktadır. Difüzyon, iyon implantasyonu, litografi, dağlama ve metalizasyon işlemleri gibi temel hususlar ele alınmaktadır. Bu imalat yöntemleri, seri üretimin fizibilitesinin yanı sıra grafen bazlı ISFET biyosensörün güvenilirliğini de sağlar. Bu bölümde, bu yöntemlerin elektronik, fotonik, MEMS (Mikroelektromekanik Sistemler) ve diğer alanları ilerleten karmaşık mikro cihazlar oluşturmak için nasıl kullanıldığını keşfediyoruz. Tarihsel olarak, işleme prosesleri olarak sınıflandırılan mikrofabrikasyon yöntemleri, entegre devrelerin üretiminde kullanılmıştır. Temel süreçler, substratın temizlenmesini, çeşitli biriktirme teknikleri kullanılarak ince bir film bırakılmasını, litografik teknikler kullanılarak maske malzemesinin bırakılmasını, mikro ölçekli özellikler için gerekli şekilleri oluşturmak için aşındırmayı, kimyasal veya plazma dağlama kullanarak maske malzemesinin çıkarılması ve son olarak oluşturulan yapının doğasının karakterize edilmesi Bu bölüm, mikrofabrikasyon yöntemlerinin yeni doğasına ışık tutan kapsamlı bir referans görevi görür.

Grafen bazlı çift kapılı nanoyapılı ISFET biyosensör için önerilen tasarım Bölüm 6'da sunulmaktadır. Bölüm, önerilen ISFET'in yapısını ve yöntemini açıklar ve biyosensörü geliştirmek için gereken mikrofabrikasyon prosedürlerini gözden geçirir. Ayrıca, ithal edilecek fabrikasyon cihazın parametrelerinin başka bir simülasyon ortamına nasıl çıkarılacağını gösterir, TCAD Silvaco yazılımı hassasiyet gibi gerekli analizi yapmak için kullanılır, simülasyon sonuçları, biyomoleküllerin saptanmasında grafen bazlı biyosensörün performansını ve etkinliğini gösterir. TCAD Silvaco simülasyonlarının sağladığı dinamik içgörülerle birlikte çift kapılı yapının karmaşık mimarisi ortaya çıktı. Bu aşama, titizlikle yetiştirilen inovasyonun somut bir temsili olan teori ve uygulamanın kaynaşmasını temsil eder.

Sensör sinyallerini faydalı verilere dönüştüren önemli bir parça olan okuma devresinin tasarımı, modellenmesi ve analizi Bölüm 7'de ele alınmıştır. Bu bölüm Cadence Virtuoso'ya genel

bir bakış sunuyor ve ISFET ve elektrolit modellerinin nasıl geliştirildiğini anlatıyor. Üçüncü bölüm, MOSFET diferansiyel amplifikatörünü açıklar, biyosensörün sinyallerini çıkarmak, yükseltmek ve anlamlı verilere çevirmek için gereken titiz sanatı kapsar. Tasarım, modelleme ve kapsamlı Cadence simülasyonları ile bu bölüm, biyosensörün performansını artırmak için hassas amplifikasyon ve gürültü azaltmanın nasıl birleştiğini göstermektedir. Kadans simülasyonları, duyarlılık analizi, doğrusallık testi, stabilite analizi ve sıcaklığa bağımlılık testi de dahil olmak üzere analiz edilecek bir dizi farklı yönü sunmak için kullanılır.

Bu tezin sayfaları Sonuçlar bölümünde doruğa ulaştığından, araştırmanın önemi yankılanmaktadır. ISFET'lerin zorlukları ve fikirleri, etkilerini azaltmak için ortaya çıkan stratejilerle kafa kafaya karşı karşıya kalmıştır. Sıcaklık ve ışık hassasiyetleri, bir kez barikatlar, şimdi gelecekteki keşif ve iyileştirme için fırsatlar olarak duruyor.

Gelecekteki çalışmalar vaatle çağırıyor. Yolculuk, gelişmiş malzeme arayüzleri, geliştirilmiş mikrofabrikasyon teknikleri ve daha sofistike okuma devresi arayışı ile devam ediyor. Her zamankinden daha fazla hassasiyet, seçicilik ve gerçek zamanlı yetenek arayışı, bir sonraki aşamanın temelini oluşturur. Nanoteknoloji, malzeme bilimi ve elektrik mühendisliği alanları birleştikçe, paradigmayı değiştiren biyosensing teknolojilerinin potansiyeli daha keskin bir odak haline geliyor.

Araştırma bulgularının ve sonuçlarının bir özeti Bölüm 8'de verilmiştir. Hassasiyeti ve seçiciliği geliştiren grafen bazlı çift kapılı nanoyapılı ISFET biyosensörün tasarımının ve simülasyonunun başarılı bir şekilde uygulanması, bu tezin katkılarını oluşturmaktadır. Graphenin bir kanal malzemesi olarak etkin entegrasyonu ve önerilen çift kapılı nanoyapı tasarımı ile gelişmiş biyo-duyarlı uygulamalar mümkün olmaktadır. Biyosensörün belirli biyomolekülleri tespit etmek için performansının ve verimliliğinin daha da optimizasyonu ve taşınabilir cihazlara entegrasyon, bakım noktası uygulamaları için umut vaat ettiğini göstermektedir.

Sonuç olarak, bu tez disiplinlerarası işbirliği ve yorulmak bilmeyen soruşturmanın bir kanıtıdır. Graphene Tabanlı Çift Kapı Nanoyapılı ISFET Biosensor akademik bir arayıştan daha fazlasıdır — toplumun iyileştirilmesi için bilim ve teknolojiden yararlanmak için amansız bir sürüşte bir kilometre taşıdır. Bu araştırma bölümü sona erdiğinde, biyosensinin geleceğini şekillendirecek heyecan verici yenilikler ve keşifler vaat eden yeni bir bölüm açılıyor.grafen bazlı çift kapılı nanoyapılı ISFET biyosensörün tasarımı ve simülasyonu biyosensör teknolojisi alanını geliştirir. Hassas ve seçici biyomoleküler tespit için yeni fırsatlar, grafenin başarılı bir şekilde entegrasyonu ve önerilen çift kapılı mimari ile mümkün olmaktadır. Grafen Tabanlı Çift Kapı Nanoyapılı ISFET Biosensor, akademik bir arayıştan daha fazlasıdır —, insan yaratıcılığının, merakının ve toplumun iyileştirilmesi için amansız bilgi arayışının bir kanıtıdır. Gelecekteki araştırmacılar, tıbbi, çevresel izleme üzerinde faydalı bir etkiye sahip olacak grafen bazlı biyosensörleri araştırmak, geliştirmek ve geliştirmek için bu çalışmadan elde edilen bilgilerle motive edilecektir, ve biyoteknolojik uygulamalar.

ACKNOWLEDGEMENTS

Praise and thanks to Allah first and foremost whose blessing enabled me to accomplish this project.

We wish to express my deepest appreciation to our supervisor DR. Mustafa ISTANBULLU for relentless guidance, helpful suggestion, close supervision and moral encouragement to complete this task.

It has been a great learning experience working under the guidance of DR. Mustafa ISTANBULLU. His patient advice, mentorship and support have helped me to achieve my goal in a steady and progressive manner.

I would like to thank my committee members Prof. Dr. Mutlu AVCI and Assoc. Prof. Dr. Mahmud Yusuf TANRIKULU for taking the time and reviewing my studies during the MSc.

I would like to thank Assoc. Prof. Dr. Ahmet EKİCİBİL and Prof. Dr. Mutlu AVCI for giving a chance to attend their amazing solid-state physics and Integrated circuits courses.

Last but not the least; I would like to express my deepest gratitude to my parents, Waheeb and Jamila HARB for their patience and support despite the distance. I also thank my brothers and sisters for their continuous support.

Our Lord! Grant us from Yourself mercy and prepare for us from our affair right guidance.

LIST OF TABLES

Table 3.1. Sensitivity of the ISFET with different sensing films. 14
Table 3.2. ISFETs with different gate structures 15
Table 5.1. Properties of metals for the metallization process 31
Table 6.1. Structural simulation parameters. 34
Table 6.2. Structure materials and their lattice constants 34
Table 6.3. properties of deposited polysilicon and germanium layers 36
Table 6.4. Extracted parameters and used ATHENA code 39
Table 6.5. Sensitivity of front-gate scanning for different sensing films. 41
Table 7.1. The editable parameters and properties of the developed Gr-ISFET model 44
Table 7.2. Parameters and physical quantities. 45
Table 7.3. Parameters used in the electrolyte model and their physical meaning 46
Table 7.4. Design specifications of the differential amplifier 49

LIST OF FIGURES

Figure 3.1. Basic structure of ISFET 10
Figure 3.2. A representation of ISFET and analogy to MOSFET 11
Figure 3.3. Dissolved free ions surrounded by water molecules 12
Figure 4.1. Simplified Energy Momentum Diagram of Graphene 20
Figure 4.2. Schematic of Graphene-based FET 20
Figure 5.1. Standard micromachining flow chart 23
Figure 5.2. Typical fabrication process for an integrated circuit (IC) 24
Figure 5.3. (a) interstitial Diffusion; (b) substitutional/vacancy Diffusion 26
Figure 5.4. (a) Implantation with resist mask and (b) dopant profile in ion implantation 27
Figure 5.5. Basic steps of photolithography 29
Figure 5.6. Wet etching and dry etching 30
Figure 6.1. a) Block diagram and b) constructed structure of graphene based ISFET in Silvaco. 33
Figure 6.2. Density of states NC and NV versus pH values. 35
Figure 6.3. ISFET Flow chart of ISFET microfabrication 36
Figure 6.4. Substrate structure and doping concentration 37
Figure 6.5. Structure and doping concentration after well oxidation 37
Figure 6.6. Structure and doping concentration after graphene deposition 38
Figure 6.7. ISFET structure after sensitive layer deposition 38
Figure 6.8. ISFET structure and doping concentration after electrolyte deposition 38
Figure 6.9. Final ISFET structure and doping concentration after metallization 39
Figure 6.10. a) $ID - VD$ and b) $ID - VG$curves of the proposed device. 40
Figure 6.11. ISFET transfer characteristics with different pH values 41
Figure 7.1. Gr-ISFET instance in Cadence virtuoso 44
Figure 7.2. (a) Electrolyte model (b) Representation of a pH sensor 45
Figure 7.3. Proposed ISFET readout circuit 47
Figure 7.4. Basic MOSFET differential amplifier circuit 48
Figure 7.5. Sensitivity of the proposed device with pH value 4,7 and 10 50
Figure 7.6. Linearity of the proposed device 51
Figure 7.7. Stability analysis of the proposed device with pH value 4,7 and 10 52
Figure 7.8. Temperature-dependency with pH value 4,7 and 1 52

SYMBOLS AND ABBREVIATIONS

ISFET	: Ion-Sensitive Field-Effect Transistor.
MOSFET	: Metal-Oxide-Semiconductor Field-Effect Transistor.
CMOS	: Complementary Metal-Oxide-Semiconductor.
IC	: integrated circuit.
GFET or Gr-ISFET	: Graphene Ion-Sensitive Field-Effect Transistor.
FET	: Field-Effect Transistor.
TCAD	: Technology Computer Aided Design.
DNA	: Deoxyribonucleic acid.
DC	: Direct current.
DOC	: Density of States.
MEMS	: Microelectromechanical Systems.
EDA	: Electronic Design Automation.
DRC	: Design Rule Checking.
EUV	: Extreme Ultraviolet.
RIE	: reactive ion etching.
PVD	: physical vapor deposition.
CVD	: chemical vapor deposition.
PR	: Photoresist.
AIS	: Active ISFET Sensor.
CIMP	: Complementary ISFET MOSFET Pair.
FESEM	: Field emission scanning electron microscopy
EDS	: Ehlers-Danlos syndromes.
XRD	: X-Ray diffraction analysis.

1. INTRODUCTION

The field of biosensors has made significant advancements in recent years, and it has become a promising field for numerous applications in biotechnology, environmental monitoring, and healthcare. Ion-Sensitive Field-Effect Transistors (ISFETs), one of the various biosensor technologies, have attracted considerable attention because of their sensitivity, label-free detection abilities, and compatibility with miniaturization for point-of-care diagnostics.

ISFET is a type of sensor that can measure the concentration of ions in a liquid. The sensor consists of a tiny semiconductor chip covered with a thin layer of material sensitive to ions. When ions in the liquid come into contact with this layer, they change the electrical properties of the chip, which can be measured and translated into a numerical value indicating the concentration of ions present (Bergveld, 2003). ISFET sensors are commonly used in medical and environmental applications, such as monitoring the pH levels of blood or measuring the acidity of water samples. They are preferred over traditional glass pH sensors since they are more durable, less prone to damage, and can be made smaller for compact devices.

A graphene-based ISFET typically consists of a thin layer of graphene that is deposited onto a substrate, such as silicon dioxide. The graphene layer is then coated with a material that is sensitive to ions, such as a polymer or metal oxide. The top of the sensing layer is gate electrode, which is separated from the graphene layer by a thin insulating layer, such as silicon dioxide. The gate electrode is used to control the flow of electrical current through the graphene layer, and the insulating layer prevents direct contact between the gate electrode and the sensing layer.

When ions in a liquid come into contact with the sensing layer, they change the electrical properties of the graphene layer, which can be detected and measured by the transistor. By controlling the voltage applied to the gate electrode, the electrical properties of the graphene layer can be modulated, allowing for precise control and measurement of ion concentrations in the liquid.

The aim of this thesis is to design and simulate a novel dual-gate nanostructured ISFET biosensor that takes advantage of graphene's unique characteristics as a channel material. The extraordinary electrical, mechanical, and chemical properties of graphene, a single layer of carbon atoms arranged in a two-dimensional honeycomb lattice, make it a suitable material for sensitive bio-detection.

ISFET biosensors possess much potential; however, current technologies still have many challenges. Conventional ISFET sensors may be affected by biofouling or fouling effects, have low sensitivity, and pH interference. The sensitivity and selectivity of ISFET biosensors can be improved using nanoscale engineering, specifically by using graphene as the channel material and sapphire as the sensing material. This research aims to address the limitations of conventional devices and create a platform for highly effective and dependable biosensing by designing a dual-gate nanostructured ISFET biosensor.

Graphene-based ISFETs offer several advantages over traditional ISFETs. Graphene is an excellent electrical conductor, allowing faster and more accurate detection of ion concentrations (Islam, 2017). Additionally, graphene is extremely thin and flexible, making it suitable for use in various applications, including wearable devices and sensors that can be integrated into clothing or other materials. Overall, graphene-based ISFETs have the potential to improve the accuracy, sensitivity, and durability of ion sensors, leading to new opportunities for sensing applications in fields such as biomedical and medicine.

The characteristics of materials and their structural properties determine the device outcomes. Dimensions of the gate terminal and the sensing film affect the device's performance. Remarkably, researchers in their studies concentrate on the sensing layer of the ISFET, including silicon dioxide (SiO_2), tantalum pentoxide (Ta_2O_5), aluminum oxide (Al_2O_3), and silicon nitride (Si_3N_4).

The electrolyte model and device are designed and simulated using the Silvaco TCAD tool, as described in the study of (Choksi et al. 2017b). In the related work, the (Al_2O_3)-based ISFET has a sensitivity of 59.172 mV/pH, slightly higher than the Nernstian limit (59 mV/pH). Compared to (SiO_2) and (Si_3N_4), ISFETs with (Al_2O_3) sensing films have greater sensitivity. Changing the sensing films leads to threshold voltage variations and sensitivity for a specific pH value. These changes are due to variations in electrochemical parameters like surface site density and dissociation constants. Sensitivity also varies according to the thickness of the sensing film, with thinner films leading to increased sensitivity.

Designing and simulating a graphene-based dual-gate nanostructured ISFET biosensor with superior sensitivity and selectivity for particular biomolecular detection is the primary goal of this study. The specific objectives of the study are as follows:

1. To review the state-of-the-art ISFET biosensors, highlighting their applications and limitations.
2. To explore the exceptional properties of graphene as a sensing material and its advantages over conventional materials used in ISFET biosensors.
3. To investigate the microfabrication process required to integrate graphene into a dual-gate nanostructured ISFET biosensor, ensuring compatibility with standard semiconductor manufacturing techniques.
4. To propose and optimize the design of the dual-gate nanostructured ISFET biosensor, considering the requirements for biomolecular detection and device performance.
5. To design a readout circuit that can efficiently translate the electrical signals from the biosensor into meaningful data, and to analyze its performance through simulations.

This thesis will be organized into eight chapters to present a comprehensive study on the design and simulation of a graphene-based dual-gate nanostructured ISFET biosensor. Chapter 2, "Preliminary Work", will provide an overview of the fundamental concepts and existing research related to ISFET biosensors, graphene, and biosensing techniques. Chapter 3, "ISFET Biosensors", will discuss the principles of ISFET operation, its applications, and the challenges faced in biomolecular detection. Chapter 4, "Graphene", explores the remarkable properties of graphene that make it an attractive material for biosensing applications.

Furthermore, Chapter 5, "Microfabrication Process", will focus on the fabrication techniques involved in integrating graphene into the ISFET biosensor and ensuring device reliability. Moving to Chapter 6, "Design of Graphene-Based Nanostructured ISFET Biosensor", which will present the proposed design of the dual-gate nanostructured ISFET biosensor and its optimization. Chapter 7, "Readout Circuit: Design, Modelling, and Analysis", will focus on the design and analysis of the readout circuit using the Cadence Virtuoso environment. This readout circuit converts sensor signals into useful data. Finally, the "Conclusions", in chapter 8, will summarize the research findings and outline future directions for developing graphene-based biosensors.

This introductory chapter has provided an overview of the background, motivation, objectives, scope, and organization of this thesis. The subsequent chapters will discuss the specific aspects of ISFET biosensors, graphene, microfabrication processes, and the proposed dual-gate nanostructured ISFET biosensor's design and simulation. The study aspires to significantly contribute to the field of biosensing technology, opening new avenues for advanced biosensor development.

2. PRELIMINARY WORK

This chapter reviews the existing literature on pH sensors, specifically focusing on graphene-based dual-gate ion-sensitive field-effect transistors (ISFETs). The review aims to provide a comprehensive understanding of the advancements, challenges, and potential applications of this technology in pH sensing.

2.1. Introduction

This chapter will overview of the literature review, focusing on the context and significance of pH sensors with graphene-based dual-gate ISFETs. pH sensing plays a critical role in various fields, including environmental monitoring, biomedical diagnostics, and industrial processes. Conventional pH sensing technologies, such as glass electrodes and chemically modified electrodes, have limitations in terms of sensitivity, selectivity, and miniaturization. This necessitates the exploration of alternative sensing platforms with improved performance. Graphene, a two-dimensional carbon material, has emerged as a promising candidate due to its exceptional properties, such as high electrical conductivity, chemical stability, and large surface area. By integrating graphene with ion-sensitive field-effect transistors (ISFETs), a new class of pH sensors with enhanced sensitivity and selectivity can be realized.

2.2. pH Sensing Technologies

Before delving into graphene-based dual-gate ISFETs, it is essential to explore the different pH sensing technologies. This section presents an overview of conventional pH sensors, such as glass electrodes, ion-selective field-effect transistors (ISFETs), and chemically modified electrodes. The strengths and limitations of these technologies are discussed, highlighting the need for highly sensitive and selective pH sensors.

Kumar et al. (2015) provide a review of various soil pH detection theories, methods, and technologies. A key component of soil pH detection methods and technologies is soil pH. Soil pH is a crucial factor in crop productivity; consequently, its spatial variation is a factor in crop productivity; consequently, its spatial variation should be adequately addressed to enhance the management system for precision agriculture. Plant growth is impacted by the physical, chemical, and biological aspects of the soil as well as its pH. To determine how much fertilizer to apply to a field, soil pH, a measurement of hydronium ion (H+) concentration, is traditionally tested in laboratories. Because laboratory-based methods are insufficient, time-consuming, labor-intensive, and expensive, the developing of quick tools that can quickly identify pH variations on a site-specific basis has become crucial.

A new fiber optic-based pH sensor probe system has been developed by (Savadjiev, 2020), It is a very promising device based on preliminary and evaluated results. The device significantly

improves sensor performance over current devices. Since the design has used small-diameter optical fibers and small tip diameters, which is crucial for monitoring the small volume samples frequently available from biological or clinical work, highly accurate pH measurements are now possible using very small volumes. The developed pH sensors are extremely stable over time when combined with the newly developed signal processing equipment.

2.3. Ion-Sensitive Field-Effect Transistors (ISFETs)

ISFETs are a class of devices that operate based on the field effect modulation caused by changes in the ion concentration in the sensing solution. This section provides an overview of ISFETs and their operation principles. The discussion includes the structure, working mechanism, and the importance of gate dielectric in ISFET-based pH sensors.

In (Sinha et al. 2021), an AlN-gate ISFET pH sensor design, modeling, fabrication, and characterization are reported. The related study optimized the AlN sensing film deposition process to achieve the desired stoichiometry. The effects of various process variables on the development of the film were carefully examined. The stoichiometry and surface morphology of the sensing film were determined using FESEM (Field emission scanning electron microscopy) and XRD (X-Ray diffraction analysis) techniques. The sensitivity of the manufactured device was obtained as 33 mV/pH. In order to validate the experimental findings, an ISFET behavioral macro model was also constructed in the SPICE environment, and the impact of various electrochemical parameters on device performance was discussed. Finally, it was discovered that the dissociation constant and primary amine site density for AlN sensing film significantly affects the sensitivity of the ISFET.

The electrolyte model and device are designed and simulated using the Silvaco TCAD tool, as described in the study of Choksi et al. (Choksi et al. 2017a). In the related work, the (Al_2O_3)-based ISFET has a sensitivity of 59.172 mV/pH, slightly higher than the Nernstian limit (59 mV/pH). Compared to (SiO_2) and (Si_3N_4), ISFETs with (Al_2O_3) sensing films have greater sensitivity. Changing the sensing films leads to threshold voltage variations and sensitivity for a specific pH value. These changes are due to variations in electrochemical parameters like surface site density and dissociation constants. Sensitivity also varies according to the thickness of the sensing film, with thinner films leading to increased sensitivity.

The study of Wang and Tang (Wang and Tang, 2021) introduced a novel ISFET device and investigated how using $GaAs$ as a substrate affects its sensitivity. $a-IGZO$ material was added to enhance the characteristic curve further and increase the sensitivity from three to four and a half times the Nernst limit. The sensitivity is boosted to seven times the Nernst limit by incorporating SiC materials. The study also examines the effect of different insulating layer materials on the device's sensitivity. Overall, the new ISFET structure achieved a sensitivity of approximately 12 times the Nernst limit.

2.4. Graphene-Based Dual-Gate ISFETs

Building upon the previous sections, this section focuses on the integration of graphene with ISFETs to develop pH sensors with high sensitivity. The review covers various aspects related to graphene-based dual-gate ISFETs, including fabrication methods, device structures, and their pH sensing performance. Notable studies and research efforts in this area are highlighted, emphasizing the advancements in sensitivity, selectivity, response time, and stability.

Huang et al. (2022) established a graphene-based ISFET with an ion-selective membrane that can sensitively and specifically detect sodium ions. To create the GFETs, a large-area, high-quality monolayer graphene was grown by chemical vapor deposition, followed by a scalable photolithographic process. In order to effectively capture sodium ions, the as-fabricated GFETs were next functionalized with sodium ionophore.

In our previous study (Harb and Istanbullu, 2022), the front gate sweeping analysis was performed for the proposed ISFET device and 55 mV/pH of sensitivity which is less than the Nernst limit was achieved. In the related study, the influence of channel parameters and the back gate voltage on the device performance are also analyzed.

2.5. Challenges and Future Directions

While graphene-based dual-gate ISFETs hold great promise for highly sensitive pH sensing, there are still challenges to overcome. This section discusses the current limitations, such as graphene synthesis techniques, device scalability, signal-to-noise ratio, and long-term stability. Additionally, potential strategies and future research directions are proposed to address these challenges and further enhance the performance of graphene-based dual-gate ISFETs.

2.6. Conclusion

This work proposes a graphene-based, dual-gate, ultra-sensitive ISFET device for pH sensing. Structure materials and device dimensions are modified to achieve better performance, and then electrical characteristics, performance, and sensitivity analysis are performed. SILVACO TCAD environment is used to run the simulations. The chemical reactions occurring at the electrolyte-insulator interface cannot currently be modeled by TCAD software. However, transport equations for the carriers in a semiconductor and the ions in an equilibrium electrolyte solution are similar. This similarity provides a solution for modeling electrolytes in the simulation environment. Therefore, a monovalent electrolyte can be represented as a semiconductor (Choksi et al. 2017a). This study uses the electrolyte, defined as a semiconductor-like layer, to test the proposed ISFET structure. Finally, results are compared with the literature, and high sensitivity and performance are observed, which validates the proposed model.

3. ISFET BIOSENSORS

3.1. Introduction and history of ISFET

Since Bergveld first created the ion-sensitive field-effect transistor (ISFET) in the 1970s as an electronic sensor for pH variations and ionic concentrations (Lu, Hou and Pan, 2018), it has several benefits in terms of mass production, quick response, easy miniaturization, and compatibility with conventional complementary metal-oxide-semiconductor technologies. The basic structure of an ISFET device is derived from the design of metal-oxide-semiconductor field-effect transistors, in which the gate electrode was changed to include a reference electrode, a chemically sensitive membrane, and a solution. The electrolyte/oxide interface's surface charge state and electrical potential can change due to the interaction between ions and amphoteric surface sites on the surface, which can change the electrical current passing through the semiconductor channel.

Silicon dioxide was the first ion-sensing membrane to be used. Simply because it is a typical gate insulator and resembles the glass electrodes that have traditionally been used to measure pH. It was discovered to be sensitive to a solution's proton (H+) concentration or pH. Various insulator materials have been demonstrated to produce a range of pH sensitivities (Al-ahdal, 2012). The ISFET gains ion selectivity by covering the oxide gate insulator with an ion-selective membrane.

Because early ISFETs lacked polysilicon gates and had unique layout specifications that made encapsulation easier, they were created using specialized MOS manufacturing techniques. Since 1999, it has been used to produce ISFETs due to the low-cost mass production of conventional CMOS (Complementary Metal-Oxide-Semiconductor) processing [7]. This had additional benefits since the sensor's driving circuitry and pre-processing blocks could be included in the same integrated circuit (IC). Additionally, ISFET arrays could be constructed, enabling a variety of applications, including lab on a chip.

ISFETs exhibit a number of non-idealities. They have temperature and light sensitivities. These shorten its lifespan and contribute to its hysteresis. These issues, however, are not as severe as they appear. There are strategies for handling them. For example, Temperature Compensation, it involves incorporating temperature sensors alongside ISFETs to monitor the ambient temperature. The ISFET's output can then be adjusted based on the temperature reading to correct for any temperature-induced deviations.

3.2. ISFET working principle

The Ion-Sensitive Field-Effect Transistor (ISFET) is a solid-state biosensor widely used in various applications due to its high sensitivity and compatibility with microfabrication techniques. The working principle of an ISFET is based on the modulation of the electrical characteristics of a field-effect transistor (FET) by changes in the surface potential induced by ion concentration variations in a solution. The ISFET consists of a metal oxide semiconductor (MOS) gate exposed to

the analyte solution, source-drain terminals for current flow, and a substrate acting as a reference electrode. When the analyte solution interacts with the gate surface, ions in the solution generate an electric double layer, resulting in a shift in the gate voltage (Elyasi and Jamasb, 2018). This voltage shift changes the conductance of the transistor, allowing the detection and quantification of the target analyte. Figure 3.1 describes the basic structure of the ISFET. The relationship between the gate voltage (V_G) and the ion concentration (C) can be described by the Nernst equation, which relates the ion concentration to the equilibrium potential.

$$V_G = V_0 + S * \log (C / C_0) \quad (3.1)$$

where, V_G is the gate voltage, V_0 is the equilibrium potential at a reference concentration C_0, S is the slope of the Nernstian response, and C is the concentration of the target ions. This equation determines ion concentration by measuring the corresponding gate voltage shift, enabling sensitive and selective detection in ISFET biosensors.

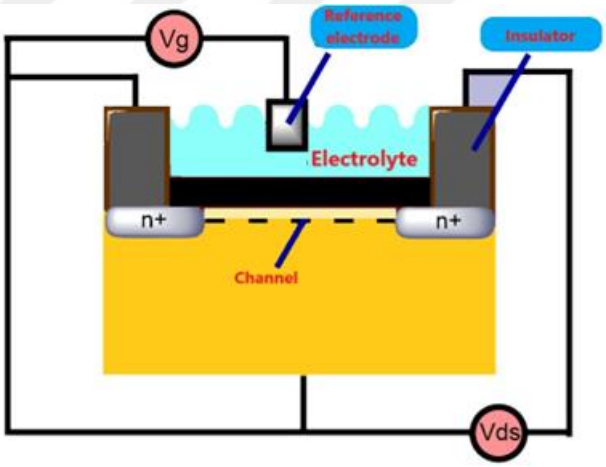

Figure 3.1. Basic structure of ISFET

3.3. ISFET and MOSFET: Basic Analogy

This section presents a concise overview of the fundamental analogy between the Ion-Sensitive Field-Effect Transistor (ISFET) and the Metal-Oxide-Semiconductor Field-Effect Transistor (MOSFET). The ISFET, a crucial device in biosensing applications, shares several fundamental principles with the widely employed MOSFET. Both transistors operate based on the modulation of charge carriers in a semiconductor channel with the electric field established by a gate electrode. By understanding the parallels between ISFET and MOSFET architectures, we can leverage existing knowledge from MOSFET technology to enhance the design and performance of ISFET-based biosensors, opening up new avenues for improved sensing capabilities and analytical accuracy.

Figure 3.2 shows a cross-section of a similar-type ISFET and MOSFET. It demonstrates how gate oxide transforms into an ion-sensitive membrane. To increase ion selectivity, additional materials may be used or layered on top of it (Al-ahdal, 2012). In essence, this is how this structure varies from the typical MOSFET. As a result, the MOSFET model is considered a starting point for ISFET modelling.

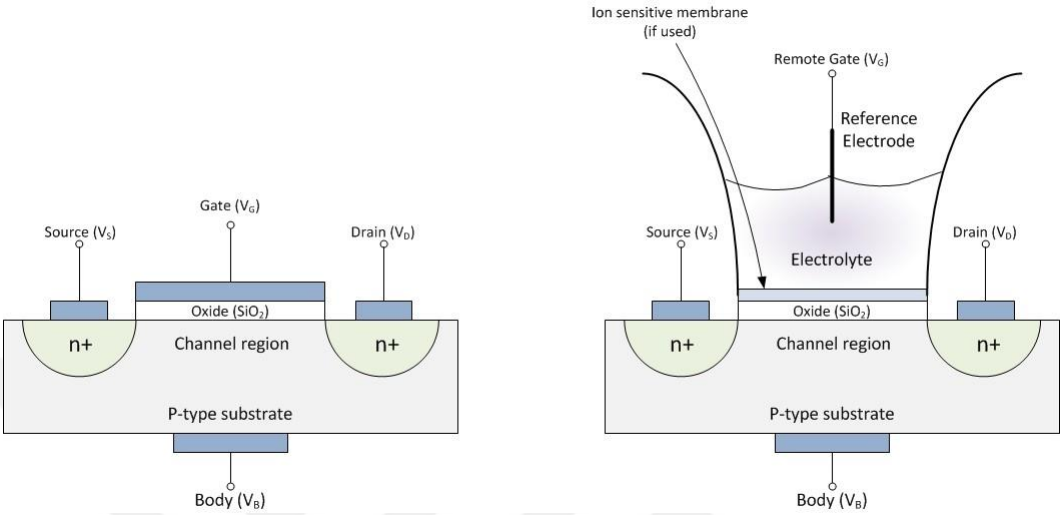

Figure 3.2. A representation of ISFET and analogy to MOSFET (Al-ahdal, 2012)

The gate material, substrate doping, insulator, and the charges in this system determine the MOSFET's threshold voltage. On the other hand, in ISFET, the electrolyte can be considered a part of the system. Therefore, the ISFET's threshold voltage becomes dependent on the properties of the electrolyte.

3.4. Electrochemistry of Ionic Solutions (Electrolytes)

In electrolytes (ionic solutions), chemical compounds or ion activity (concentration) are investigated. Chemical compounds are dissolved in polar solvents, like water, to create these solutions. Since its molecules are not symmetrically charged, water is one of the most widely used solvents. Consequently, water has a particular dipole moment. The compounds' chemical bonds are weakened by this dipole moment, which causes them to dissolve. Ions that have been dissolved are encircled by enough water molecules to screen their charge (Y. C. Wu and Lin, 2015).

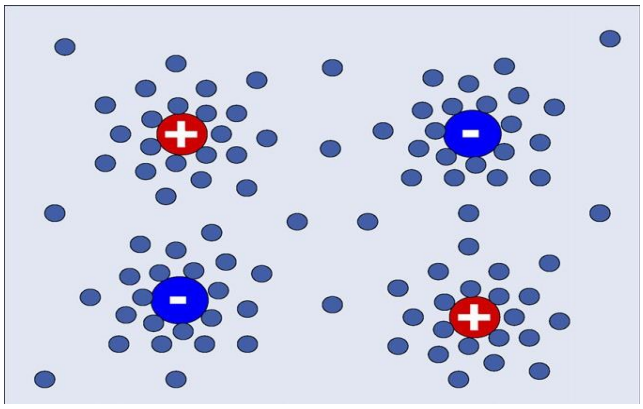

Figure 3.3. Dissolved free ions surrounded by water molecules (Baylay, 2010)

Through this mechanism, the ions are shielded from the effects of the surrounding electric fields by a change in the dielectric constant. As a result, the ions are now free to move around in the solution and carry current. This mechanism for an electrolyte with free ions of dissolved salt is illustrated in Figure 3.3.

3.5. Concept of pH (Power of Hydrogen)

The measurement of pH is crucial in various applications, including ISFET biosensors. Traditional pH measurement methods involve using pH meters equipped with glass electrodes. The glass electrode generates a potential difference proportional to the hydrogen ion concentration, enabling accurate pH measurements in various solutions. ISFET biosensors are devices that utilize pH-sensitive ISFETs to detect changes in the pH of a solution, which can be indicative of specific biological or chemical events. The pH-sensitive ISFET consists of a metal-oxide-semiconductor field-effect transistor (MOSFET) with a pH-sensitive gate material, typically silicon nitride (Si_3N_4). When the solution's pH changes, it alters the surface charge of the gate material, causing a shift in the ISFET's threshold voltage (Vth) (Tian et al. 2015a).

As given in Equation 3.1, The pH of a solution is a measure of the concentration of hydrogen ions (H^+) in the solution. It is defined as the negative logarithm of the hydrogen ion concentration:

$$pH = \log [H^+] \qquad 3.2)$$

where $[H^+]$ represents the concentration of hydrogen ions in moles per liter (mol/L) or molarity (M).

The relationship between the threshold voltage shift (ΔVth) and the change in pH (ΔpH) is typically described by the Nernst equation is given by Equation (3.2):

$$\Delta Vth = S \times \Delta pH \qquad 3.2)$$

where S is the sensitivity of the ISFET, representing the change in threshold voltage per unit change in pH.

In electrolytes, the water molecules partially dissolve in addition to the chemicals. The following equation controls this mechanism and it eventually finds equilibrium:

$$H2O \rightarrow H^+ + OH^- \quad (3.3)$$

Equation (3.4) gives the equilibrium constant for the chemical equation (3.3) in terms of molar concentrations, or moles per liter, of the species.

$$k = \frac{[H^+][OH^-]}{[H2O]} \quad 3.4)$$

3.6. pH Sensing Insulators

The pH-sensitive insulator is the most crucial component in pH measurements. It is the layer that actually interacts with the electrolyte. A good pH-sensitive insulator must exhibit a linear response over a broad pH range, high hydrogen ion selectivity, and low other ion selectivity (Baylay, 2010). It should perform with low drift and high sensitivity to changes in hydrogen ion concentration. The first pH-sensitive insulator to be applied to an ISFET was SiO_2.

This section will discuss a critical component in Ion-Sensitive Field-Effect Transistors (ISFETs) for pH measurement applications. pH sensing insulators play a pivotal role in enabling the reliable and accurate detection of pH levels in various environments. These insulators typically consist of metal oxide thin films, such as silicon dioxide (SiO_2) or aluminum oxide (Al_2O_3), which are deposited on the surface of the ISFET gate electrode. The insulator layer acts as a barrier between the analyte solution and the gate electrode, providing electrical isolation while allowing the passage of hydrogen ions (H+) from the solution to the gate insulator interface.

The pH-sensing insulator operates on the principle of the pH-dependent surface charge, where the presence of hydrogen ions alters the surface charge density at the insulator-electrolyte interface. The change in surface charge affects the electrostatics in the gate region, modifying the electrical characteristics of the ISFET. As the pH of the analyte solution varies, the gate voltage required to maintain a certain drain current changes, thereby providing a measurable electrical signal proportional to the pH value (Werner et al. 2021).

Table 3.1 summarizes the previous state of art studies of ISFET in terms of sensitivity and sensitive layer. The proposed graphene-based device presents the best sensitivity score compared to the literature.

Table 3.1. Sensitivity of the ISFET with different sensing films.

Channel material	Sensitive layer	Sensitivity	Reference
Graphene	Nano-graph.	140 mV/pH	(Jung et al. 2021)
SiGe	Al_2O_3	360 mV/pH	(Dinar et al. 2019a)
IGZO	Ta_2O_5	585.3 mV/pH	(Wang and Tang 2021)
Inp	Indium oxide	58.3 mV/pH	(Chang et al. 2011)
MoS_2	Al_2O_3	50 mV/pH	(Wei et al. 2020)
Si	Al_2O_3	51.2 mV/pH	(Nakata et al. 2017)
Si	SiO_2	152.1 mV/pH	(Mohammadi and Manavizadeh 2019)
Si	Si_3N_4	57.14 mV/pH	(Choksi et al. 2017a)
Graphene	**Al_2O_3**	**1066 mV/pH**	**Proposed study**

The selection and optimization of the pH sensing insulator material are crucial in achieving high sensitivity, stability, and selectivity in pH sensing applications. Factors such as the insulator thickness, surface functionalization, and choice of metal oxide material significantly influence the overall performance of the ISFET-based pH sensor. In recent years, material science and nanotechnology advancements developed novel pH sensing insulator materials with enhanced properties, including improved sensitivity, reduced drift, and increased robustness against fouling and interference.

3.7. Reference electrode

The reference electrode is typically composed of a stable and reversible redox couple in contact with an electrolyte solution. One of the most commonly used reference electrodes in ISFET-based pH sensors is the silver/silver chloride (Ag/AgCl) electrode. This electrode consists of a silver wire coated with a layer of silver chloride, immersed in an electrolyte solution containing chloride ions. The Ag/AgCl electrode provides a stable and reproducible potential, unaffected by changes in the pH of the analyte solution (Ma et al. 2022).

The reference electrode is connected to the ISFET circuitry, allowing the ISFET to measure the potential difference between the reference electrode and the ISFET gate electrode. This potential difference, known as the gate potential, is crucial for the accurate determination of pH. By comparing the gate potential with the reference electrode potential, the pH-sensitive ISFET can effectively convert the pH-dependent gate potential into a measurable electrical output.

To ensure accurate pH measurements, it is essential to properly calibrate and maintain the reference electrode. Calibration involves comparing the reference electrode potential against a

known pH standard to establish a calibration curve. Regular cleaning, reconditioning, and storage in appropriate electrolyte solutions are necessary to maintain the stability and accuracy of the reference electrode over time.

3.8. Gate structures

Along with the advancement of CMOS technology, there has been much interest in modifying and enhancing the gate structure of the ISFET. Here, we identify the various gate structures that support their sensing capabilities. These gate structures have a significant impact on the sensitivity, selectivity, and stability of devices used for detecting ions, pH levels, and particular biomolecules. As we proceed through this section, various gate structures will be discussed, from unmodified CMOS processed ISFETs, dual-gate ISFETs, floating and extended gate ISFETs. Table 3.2 illustrates the applications and references of the different gate structures.

Table 3.2. ISFETs with different gate structures

Gate Structure	Application	Ref.
Unmodified CMOS gate	pH and ion sensing	(Kotsakis et al. 2021)
Dual-gate	pH sensing	(C. C. Wu and Wang, 2021)
Floating-gate	DNA detection and proton imaging	(Yu et al. 2020)
Extended-gate	pH sensing	(Pullano et al. 2019)

The unmodified CMOS-processed ISFETs are based on conventional CMOS technology, where the gate is typically composed of silicon dioxide (SiO2) and doped silicon. They form the basis for pH and ion sensing, and their simplicity allows for mass production at low cost. Understanding unmodified CMOS ISFETs is essential in appreciating the advancements made in subsequent gate structures, paving the way for more sophisticated sensing capabilities.

Another typical structure is the dual-gate ISFETs, a significant advancement in sensing technology. Dual-gate structures introduce an additional gate, often referred to as the reference or compensation gate. This dual-gate configuration enhances sensitivity and compensates for various external influences, such as temperature fluctuations and other interfering ions.

Continuing on our path with floating-gate ISFETs. These structures integrate an insulated floating gate between the sensing gate and the semiconductor channel. This unique design provides excellent isolation from the surrounding environment, reducing drift and enhancing stability. Floating-gate ISFETs are particularly advantageous in bio-sensing applications, where prolonged exposure to biological fluids necessitates robust and reliable sensing performance.

As we venture further, extended-gate ISFETs are to be discussed, where the traditional gate is replaced with an external electrode connected to the electrolyte solution. This extended gate

structure enables direct exposure to the target analytes, making it highly suitable for biological and chemical sensing. The extended-gate configuration enhances sensitivity and facilitates selective measurements, making it a powerful tool in various real-time monitoring applications, such as environmental and biomedical sensing.

In this work, the dual-gate structure has been used, this kind of structures creates an additional accumulation channel, increasing the current and the subthreshold slope (Ma et al. 2022). It is possible to improve pH sensitivity by several orders of magnitude. Additionally, time drift and hysteresis performance limits in conventional ISFETs have been improved.

3.9. Biosensing applications

ISFET biosensors are essential for identifying and measuring a wide variety of biological and chemical substances. ISFET biosensors reveal their ability to change many fields, including genomics, proteomics, environmental monitoring, and healthcare, from DNA sensing and protein analysis to ion detection and microbial monitoring. This section highlights the remarkable applications of ISFET biosensors and their potential to drive innovations in personalized medicine, environmental conservation, and safer living for society.

The detection of DNA represents one of the most significant advances in biosensing. Label-free and incredibly sensitive DNA hybridization event detection is made possible by ISFET biosensors. ISFETs may quickly and effectively identify complementary DNA strands by immobilizing DNA probes on the sensor's surface, opening the door for applications in genomics, genetic testing, and customized medicine (Cacho-Soblechero et al. 2020). A new era of proactive and focused healthcare may be brought about by DNA sensing with ISFET biosensors, revolutionizing disease diagnosis, cancer screening, and infectious disease detection.

ISFET biosensors are valuable instruments for researching protein interactions and dynamics in proteomics. These biosensors are highly sensitive to detecting particular proteins or biomarkers, providing real-time information on biochemical processes and protein-binding activities. ISFET biosensors are label-free; therefore, there is no longer a need for laborious labeling procedures, creating a streamlined and effective platform for protein analysis. Proteomics has a wide range of uses, including the production of pharmaceuticals, the study of diseases, and the comprehension of intricate biological processes (Chao et al. 2020).

With their ability to quickly and precisely measure ions in a variety of environments, ISFET biosensors have been at the forefront of ion detection applications. These biosensors are excellent at identifying ions necessary for biological and environmental processes, including hydrogen ions (pH sensing), sodium and potassium (Norzin et al. 2018). ISFET biosensors can detect changes in ion concentrations in real-time by utilizing the gate sensitivity, making them essential tools for environmental monitoring, industrial process control, and physiological studies.

ISFET biosensors are used in microbial monitoring because of their high specificity and speed in detecting and identifying microorganisms. ISFET biosensors provide a label-free and quick way to identify bacteria, viruses, and other pathogens by detecting changes in pH or ion concentrations brought on by microbial metabolism (Cao et al. 2022). This ability is crucial for the early detection of microbial contamination and the facilitation of prompt interventions in the fields of food safety, water quality monitoring, and healthcare.

4. GRAPHENE

Graphene is a two-dimensional material composed of a single layer of carbon atoms arranged in a hexagonal lattice. Due to its extraordinary qualities and diverse applications, it has attracted much attention lately. The remarkable characteristics of graphene are examined in this chapter as they make it an ideal material for biosensing applications. It explores the unique electronic, mechanical, and chemical properties of graphene and shows how it can improve the performance of ISFET biosensors.

4.1. Properties of Graphene: Electronic, Mechanical and Chemical

The electronic characteristics of graphene are extraordinary. Its electrons behave as massless Dirac fermions, mimicking relativistic quantum particles, due to its linear dispersion relation near the Dirac points (Tian et al. 2015b). Because of its high electrical conductivity, graphene is an excellent option for use as a conductive channel in ISFET biosensors. Its highly mobile charge carriers produce impressive electron mobility values higher than those of conventional semiconductors. This attribute translates into faster charge transport and more sensitive detection of charge changes induced by biomolecular interactions.

The mechanical properties of graphene are incredible strength, flexibility, and lightness. One of the strongest materials known, its tensile strength surpasses that of steel. Due to its high degree of flexibility, which enables it to adapt to various surfaces, it can be used as a sensitive transducer to detect biomolecular interactions. The reliability of graphene-based biosensors is ensured by the combination of strength and flexibility, which is essential for their practical applications in a wide range of environments.

The chemical characteristics of graphene are equally impressive and support its suitability for biosensing applications. Its unusually high surface area to mass ratio provides ample space for biomolecules to interact with the graphene surface. Since functional groups are present on graphene, it is possible to be biofunctionalized, which makes it possible to detect target biomolecules with precision. An excellent candidate for bio-detection and medical diagnostics, graphene also ensures minimal interference with biological systems due to its biocompatibility (Mappes, 2022).

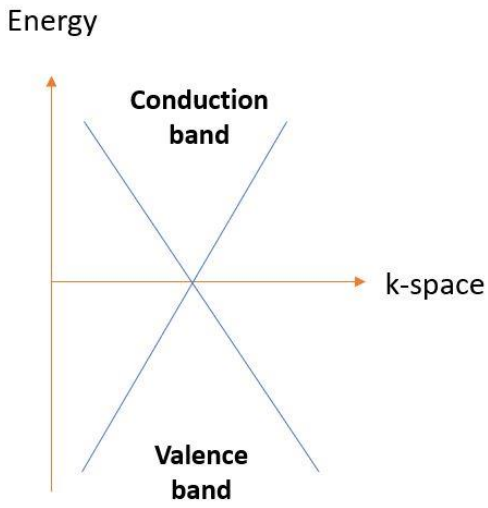

Figure 4.1. Simplified Energy Momentum Diagram of Graphene

While p-type and n-type doped regions are formed in cleanrooms for conventional semiconductors, in graphene, the doping levels can be electrically tuned in ambient conditions to conduct only holes or only electrons. The Dirac point V Dirac, the voltage at which the majority channel carrier switches from electrons to holes, or vice versa, has an impact on the presence of majority carriers at different biases. Figure 4.1 illustrates a Graphene's Energy Momentum Diagram (Trocchia,2012).

4.2. Graphene-Based Biosensors

In order to improve the performance of the Ion-Sensitive Field-Effect Transistor (ISFET) biosensor, graphene has been used as the channel material in this thesis. ISFET devices have traditionally had channels made of silicon-based materials. However, using graphene brings several advantages to the functionality of the biosensor.

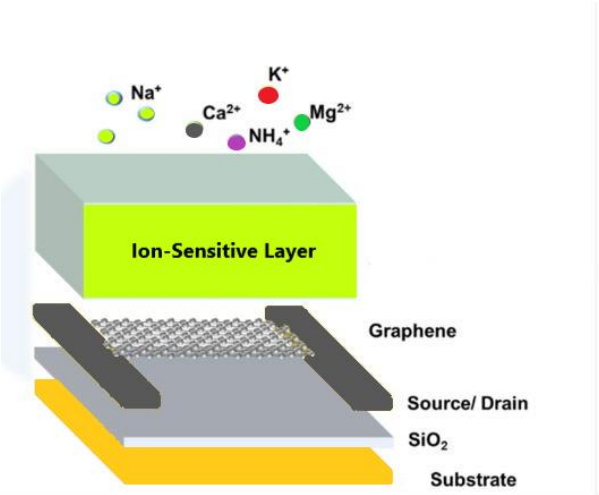

Figure 4.2. Schematic of Graphene-based FET

Since graphene is two dimensional and has a large surface area, more biomolecules can interact with the channel surface. Increased binding capacity and improved sensitivity for detecting biomolecules at low concentrations are made possible by this property. ISFET biosensors based on graphene have improved surface-to-volume ratios, which enhance bio-recognition capabilities and strengthen signal amplification.

The mechanical adaptability and light weight of graphene contribute to the biosensor's adaptability and versatility. The incorporation of graphene makes it possible to create flexible and wearable biosensor devices, expanding the range of potential applications to include point-of-care diagnostics and wearable health monitoring. The biosensor's flexibility improves its capacity to adapt to different surfaces, expanding the range of target analytes and enabling real-time, label-free biomolecular detection.

4.3. Challenges and Future Perspectives

Despite having outstanding characteristics, graphene-based biosensors have issues that need to be resolved. Scalable and reproducible graphene synthesis is one of the main obstacles. There are currently many different techniques, each with advantages and limitations, including mechanical exfoliation, chemical vapor deposition, and epitaxial growth. For graphene-based biosensors to be widely used, large-scale, cost-effective, and repeatable graphene synthesis techniques must be developed(Huang et al. 2022).

Additionally, careful thought must go into functionalizing graphene for selective biomolecular detection. For high sensitivity and selectivity in biosensing applications, the immobilization of bio-recognition components onto graphene surfaces while maintaining their electrical properties is essential.

In conclusion, graphene is a highly promising material for improving ISFET biosensors because of its exceptional electronic, mechanical, and chemical properties. Its high mechanical strength, electrical conductivity, and biocompatibility offer a solid foundation for accurate and sensitive biomolecular detection. With their ability to quickly, sensitively, and without the use of labels, graphene-based biosensors have the potential to revolutionize many industries, from environmental monitoring to medical diagnostics. However, overcoming challenges related to graphene synthesis, functionalization, and large-scale production will be vital for the practical realization of graphene-based biosensor devices. Graphene-based biosensors have the potential to lead revolutionary developments in the field of biosensing, enhancing healthcare and environmental sustainability.

5. MICROFABRICATION PROCESS

In this chapter, we will discuss the fundamental principles and advanced processes that shape the micro and nanoscale world, from the basics of microfabrication to diffusion, ion implantation, lithography, etching, and metallization processes. As we traverse through these sections, we gain insights into how these techniques are employed to fabricate intricate microdevices that advance progress in electronics, photonics, MEMS (Microelectromechanical Systems), and beyond. This chapter serves as a comprehensive guide, illuminating the transformative role of microfabrication techniques.

5.1. Basics of microfabrication

Historically, microfabrication methods, categorized as machining processes, have been used to manufacture integrated circuits. Figure 5.1 depicts the typical process used to create an integrated circuit. Any microscale product created using silicon-based materials can be produced using a similar flowchart. The diagram depicts the fundamental processes of initially cleaning the substrate, depositing a thin film using a variety of deposition techniques, depositing mask material using lithographic techniques, etching to create the necessary shapes for the microscale features, removing the mask material using chemical or plasma etching, and finally characterizing the nature of the created structure (Group, 2006).

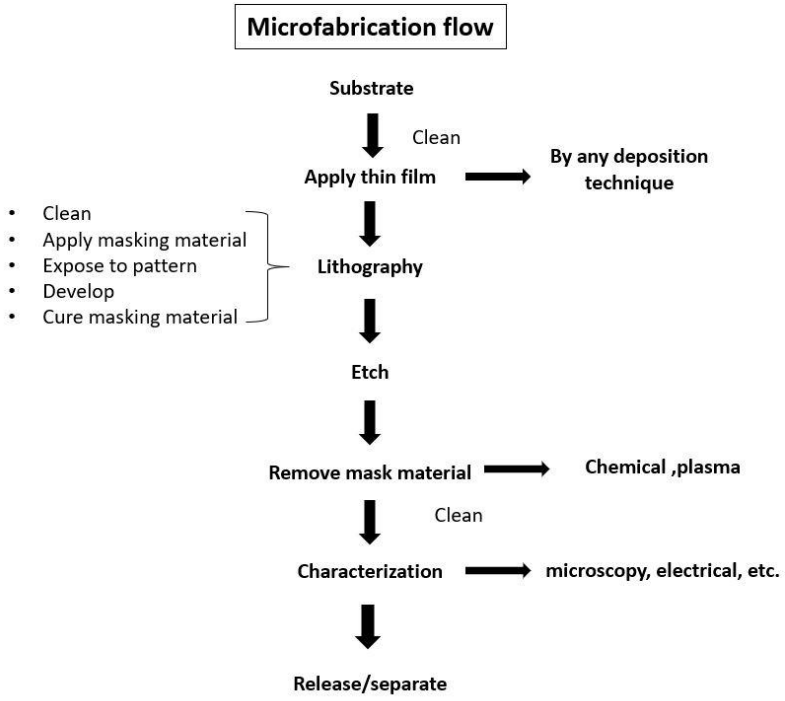

Figure 5.1. Standard micromachining flow chart

The three fundamental regimes of fabrication at the microscale are addition, multiplication, and subtraction. The substrate material is coated with a thin film during the addition phase. A thin film can be produced in an atmospheric chamber by oxidation or doping, or it can be applied to a substrate by electroplating or spraying a liquid film and allowing it to dry. Other ways include using low- and high-pressure vacuum techniques to attach a thin layer to the substrate or fusing a solid to the substrate. The creation of microscale features, especially channeled features utilized in micro- and nanofluidic systems, requires the feature multiplication process, which can take many different forms.

A number of processes, including direct writing of features utilizing electron beam, ion beam, and atomic force microscopic techniques, can be used for feature multiplication process. Along with new methods for producing micro/nanoscale features utilizing microstamping technologies, contact lithography is a common technique for depositing features. There are numerous methods for subtracting materials to form features. More than silicon, mechanical micro-milling, laser ablation, water micromachining, and numerous more methods can be used in subtraction operations. These procedures are capable of substantially higher rates of material removal.

Features of various sizes, shapes, and scales can be created by combining any of these techniques. New microfabrication techniques that improve the performance of individual devices have surpassed the traditional method of producing features on silicon.

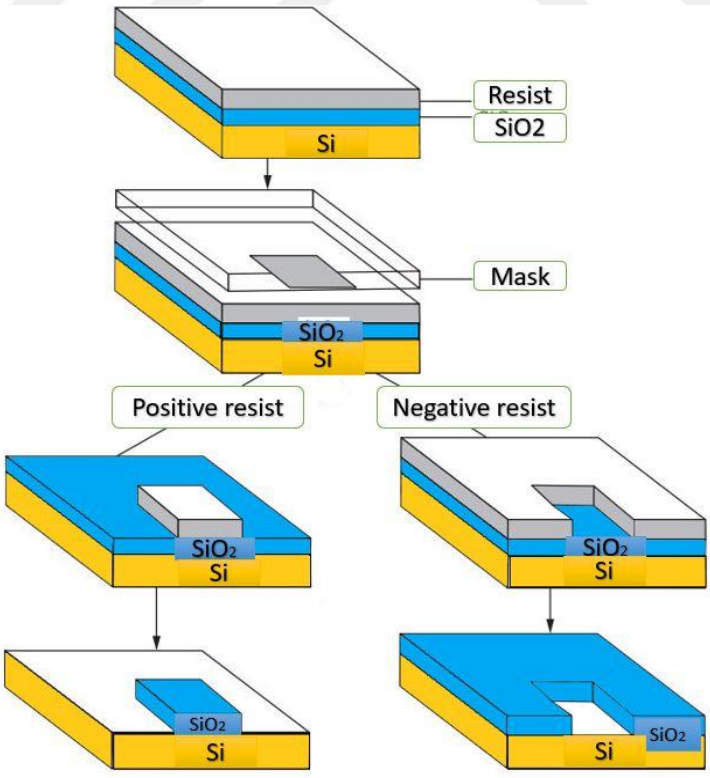

Figure 5.2. Typical fabrication process for an integrated circuit (IC)(Group, 2006).

Figure 5.2 illustrates the standard method of producing integrated circuits. It depicts the application of a thin film to the surface of silicon, which is then selectively removed using etching procedures that, owing to the texture of the silicon crystal, create wells or channels with known geometries. Bulk micromachining is the process of removing silicon from crystal planes in specific directions.

Thermal oxidation is a fundamental process in microfabrication used to grow thin oxide layers on silicon substrates. This technique plays a crucial role in the fabrication of integrated circuits, microelectromechanical systems (MEMS), and various other microdevices. Thermal oxidation involves subjecting silicon wafers to elevated temperatures in an oxidizing ambient, typically dry oxygen or steam, to form silicon dioxide (SiO2) layers.

During thermal oxidation, the process occurs at the silicon/oxide interface. Silicon atoms from the substrate combine with oxygen to form SiO_2. The oxidation rate depends on temperature, time, and oxygen availability. The oxide growth follows a linear relationship with time, known as Deal-Grove kinetics (Franssila, 2010). The oxidation rate is commonly represented by the Deal-Grove equation 5.1:

$$t_{ox} = (K \times \mathrm{t}) / \mathrm{sqrt}(1 - F) \tag{5.1}$$

where, t ox is the thickness of the grown oxide, K is the oxidation rate constant, t is the oxidation time, and F is the film stress factor.

Thermal oxidation can be classified into wet and dry oxidation, depending on the oxidizing ambient. In wet oxidation, silicon wafers are exposed to steam (H_2O) at high temperatures, typically between 800 to 1200°C. The presence of steam increases the oxidation rate compared to dry oxidation. Wet oxidation is commonly used for growing thicker oxide layers, typically ranging from several hundred nanometers to micrometers. On the other hand, Dry oxidation involves exposing silicon wafers to dry oxygen (O2) at elevated temperatures. Dry oxidation results in a slower oxidation rate compared to wet oxidation. As a result, it is suitable for growing thin oxide layers, typically in the range of a few nanometers to tens of nanometers (Group, 2006).

5.2. Diffusion

Microfabrication is a transformative manufacturing process that involves creating intricate structures and devices at the microscale level. One of the fundamental processes in microfabrication is diffusion, which plays a critical role in tailoring the electrical properties of semiconductor materials. This section explores the principles of diffusion, its types, diffusion process steps, challenges, advancements, and its pivotal applications in microfabrication.

Diffusion is the movement of atoms, ions, or molecules within a solid material, influenced by their random thermal motion. At elevated temperatures, atoms possess greater kinetic energy, leading to increased diffusion rates. The process aims to equalize concentration differences, resulting in the migration of species from regions of high concentration to low concentration. Fick's laws of diffusion mathematically describe the diffusion flux as proportional to the concentration gradient (Marc Madou, 2000).

In microfabrication, two primary types of diffusion are significant, as described in Figure 5.3. Interstitial diffusion involves the movement of smaller atoms or ions through the interstitial spaces between the crystal lattice sites of a material. For instance, hydrogen and carbon atoms in silicon can diffuse interstitially. Substitutional diffusion occurs when larger atoms or dopants replace host atoms in the crystal lattice. Dopants like boron, phosphorus, arsenic, and others in semiconductors diffuse via substitutional mechanisms.

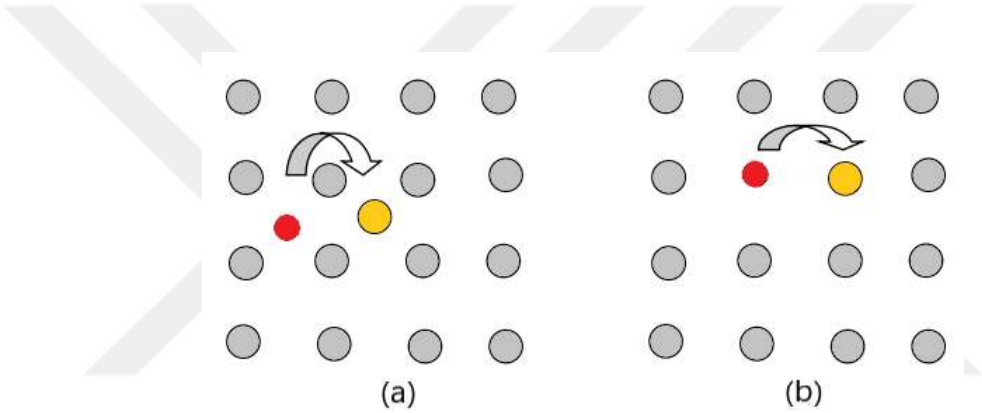

Figure 5.3. (a) interstitial Diffusion; (b) substitutional/vacancy Diffusion (Franssila 2010)

The diffusion process in microfabrication typically involves several key steps: Dopant Introduction; dopant atoms are introduced to the semiconductor material through various techniques such as ion implantation, chemical vapor deposition, or solid-state diffusion. Activation; to create the desired electrical properties, the semiconductor wafer is subjected to high-temperature annealing, which activates the dopant atoms, making them mobile for diffusion. Drive-In; during the drive-in step, the wafer is further annealed at a specific temperature and duration to drive the dopant atoms deeper into the semiconductor lattice to achieve the desired doping profile.

5.3. Ion Implantation

Ion implantation is a keystone in microfabrication due to its unrivaled precision and versatility. The process involves accelerating ions to high energies and propelling them onto a semiconductor wafer. Unlike traditional diffusion techniques, ion implantation enables precise control over the depth and concentration of dopant atoms in the material. This level of accuracy is crucial as semiconductor devices continue to shrink in size, reaching nanometer dimensions.

The heart of ion implantation lies in the ion source and its capability to generate a variety of dopant ions, including boron, phosphorus, arsenic, and many others. The ion beam current, ion energy, and dose can be finely tuned (Pares-Casanova, 2017). A wide range of silicon doping profiles can be created using ion implantation. Maximum dopant density does not necessarily have to be at the wafer surface; it can be hundreds of nanometers deep inside the silicon, see Figure 5.4. It is possible to implant through surface layers like SiO2. Thermal diffusion cannot accomplish either of these.

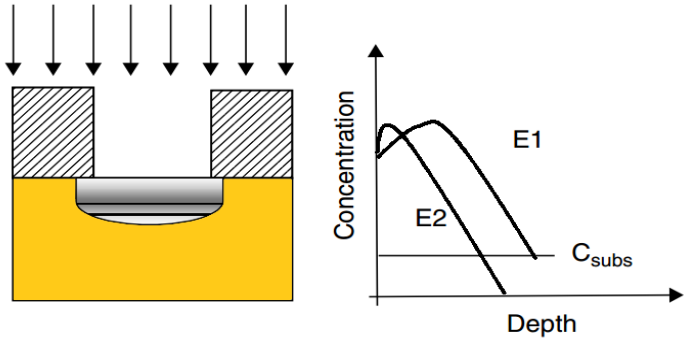

(a) (b)

Figure 5.4. (a) Implantation with resist mask and (b) dopant profile in ion implantation (Energy 1 > Energy 2)

After implantation, the wafer undergoes an annealing process, which serves a dual purpose. Firstly, it activates the dopant atoms, converting them from electrically inactive to active states. Secondly, it repairs the crystal lattice damage caused by the energetic ion impacts. This annealing step is crucial for restoring the semiconductor material's structural integrity and ensuring optimal electrical performance.

Ion implantation's contributions to microfabrication are diverse and far-reaching. In the realm of integrated circuits, the technique plays a pivotal role in creating PN junctions, the foundation of diodes and transistors. Moreover, ion implantation is the cornerstone for forming the source and drain regions in MOSFETs, a fundamental component of today's microprocessors and memory devices.

CMOS technology, which powers most modern electronic devices, owes its success to ion implantation. By selectively implanting different dopant species, engineers can engineer N-type and P-type regions, thus forming the building blocks for CMOS circuits. This versatility is instrumental in the development of high-performance and energy-efficient microelectronic devices.

The significance of ion implantation expands beyond traditional silicon-based microelectronics. In advanced compound semiconductor devices, such as gallium nitride (GaN) and silicon carbide (SiC), ion implantation has proven instrumental in tailoring their electrical properties for various applications, including power electronics and high-frequency devices. As semiconductor technology continues to advance, ion implantation remains a vital tool for researchers and engineers. Ongoing efforts focus on refining implantation equipment, optimizing ion beam profiles, and exploring novel dopant species to meet the stringent demands of nanoscale device fabrication.

5.4. Lithography

Lithography is a fundamental process in microfabrication that plays a pivotal role in defining patterns on semiconductor substrates. It involves the transfer of predefined patterns onto a substrate's surface through the use of masks and light-sensitive materials. The patterns created by lithography serve as templates for subsequent microfabrication steps, such as etching, deposition, and doping, enabling the precise fabrication of microstructures and devices.

The lithography process begins with a mask, and a transparent plate containing the desired pattern positioned in close proximity to the semiconductor substrate. The substrate is coated with a photosensitive material called a photoresist (PR). When exposed to light, the photoresist undergoes chemical changes, making it either more soluble (positive photoresist) or less soluble (negative photoresist) in a developer solution. The choice between positive and negative photoresists depends on the desired outcome of the lithography process.

During exposure, light passes through the mask, projecting the pattern onto the photoresist-coated substrate. The areas of the photoresist exposed to light become more soluble (or less soluble) and can be selectively removed during the development step. The developed photoresist pattern then acts as a protective mask for subsequent processes, such as etching or doping, transferring the pattern onto the underlying substrate. Figure 5.5 illustrates the basic steps of the photolithography process (Pares-Casanova, 2017).

1. Optical Lithography: This traditional lithography method uses ultraviolet light to create patterns on the photoresist. It is widely used in semiconductor manufacturing and can achieve sub-micrometer resolutions. However, as feature sizes in microelectronics continue to shrink, optical lithography faces challenges due to the diffraction limit.
2. EUV Lithography: Extreme Ultraviolet (EUV) lithography is an advanced technique that employs shorter wavelengths of light to overcome the diffraction limit of optical lithography. EUV lithography enables the fabrication of smaller feature sizes, making it crucial for state-of-the-art semiconductor nodes.
3. Electron Beam Lithography: Electron beam lithography uses a focused electron beam to write patterns on the photoresist directly. It offers high-resolution capabilities but can be relatively slow and expensive, making it suitable for research and low-volume production.

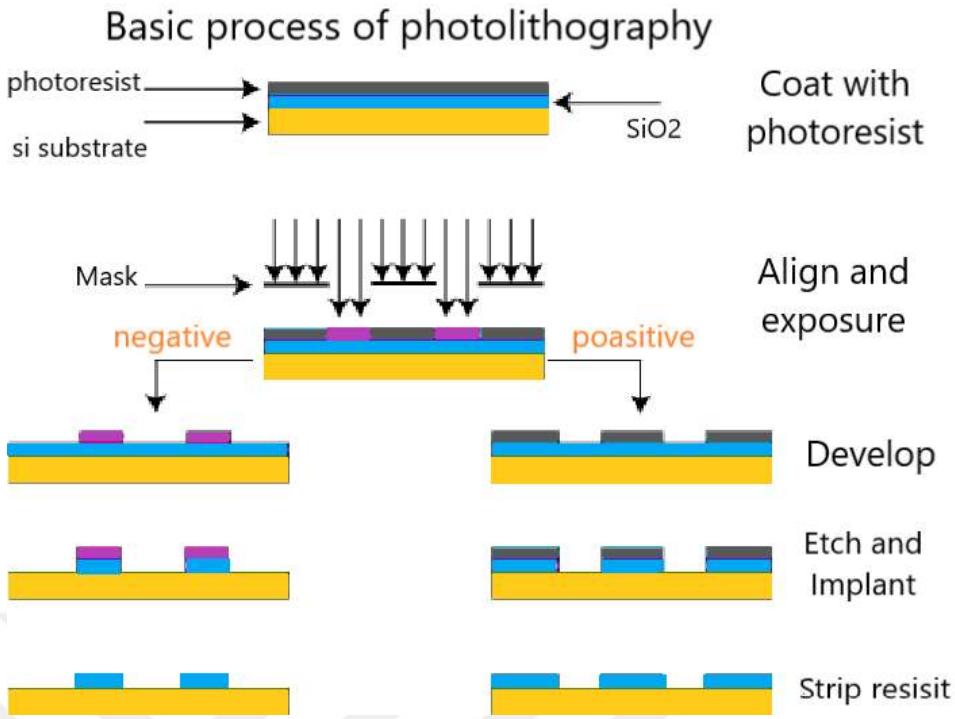

Figure 5.5. Basic steps of photolithography

Various lithography techniques are employed in microfabrication, each suited for specific applications and resolution requirements (Erismis, 2013):

4. Nanoimprint Lithography: Nanoimprint lithography involves pressing a patterned mold into a soft resist layer to transfer the pattern. It is a promising technique for high-resolution and high-throughput nanopatterning.

To conclude, lithography is a critical process in microfabrication, enabling the precise definition of patterns on semiconductor substrates. The choice of lithography technique depends on the required resolution, cost, and production volume. With continuous advancements, lithography remains a driving force behind the development of cutting-edge microelectronics and microdevices.

5.5. Etching

One of the critical processes in microfabrication, etching, is used to selectively remove material from the surface of a substrate. It also plays a central role in defining patterns and creating intricate structures on semiconductor wafers. Etching is an essential step in various microfabrication processes, including integrated circuit fabrication, microelectromechanical systems (MEMS) manufacturing, and nanotechnology.

Etching is the process of selectively removing material from a substrate to create specific patterns. It is a fundamental step in semiconductor device fabrication, where intricate structures are etched on silicon wafers to define integrated circuits' components. The process can be broadly categorized into two main types: wet etching and dry etching, as shown in Figure 5.6.

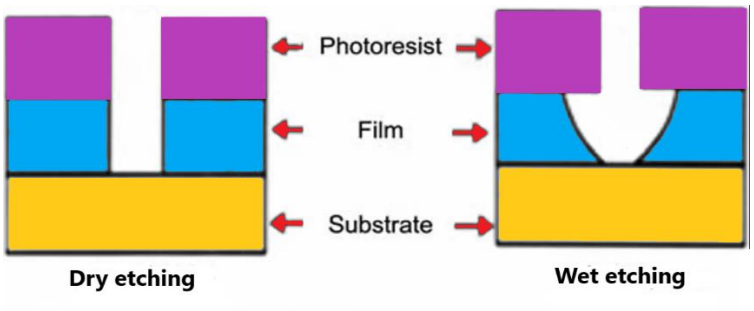

Figure 5.6. Wet etching and dry etching

Wet etching involves immersing the wafer in a liquid chemical etchant. The etchant reacts with the exposed material, dissolving it and removing it from the substrate. Wet etching is isotropic, meaning it removes material uniformly in all directions, making it suitable for simple shapes and smooth surfaces. On the other hand, dry etching is a plasma-based process that does not involve a liquid etchant. It relies on physical or chemical processes in a gaseous environment to remove material. Dry etching can be further divided into two main types: plasma etching and reactive ion etching (RIE). Dry etching is anisotropic, providing better control over feature shape and profile, making it essential for creating high-aspect-ratio structures (Marc Madou, 2000).

To understand the etching process deeply, some parameters, such as etch rate and selectivity, should be considered. The etch rate is the speed at which material is removed during etching and is typically expressed in units of nanometers per second (nm/s) or angstroms per minute (Å/min)(Franssila, 2010). It is determined by factors such as etchant concentration, temperature, and the properties of the material being etched. The etch rate can be expressed as:

$$V = k \times [\text{Etchant}] \tag{5.2}$$

where, V is the etch rate, k is the etch rate constant, [Etchant] is the concentration of the etchant.

The selectivity is the ratio of the etch rate of one material to that of another. It quantifies the degree of preference for etching one material over another. Selectivity is crucial when etching multiple materials in a single process to ensure precise pattern definition without damaging other layers. It can be expressed as:

$$S = V_{\text{material1}} / V_{\text{material2}} \tag{5.3}$$

where, S is the selectivity, $V_{\text{material1}}$ is the etch rate of material 1, $V_{\text{material2}}$ is the etch rate of material 2.

5.6. Metallization Process

The metallization process involves depositing thin metal layers, usually aluminum or copper, onto the surface of the semiconductor wafer. These metal layers serve as conductive pathways, bridging the gaps between different components and establishing electrical connections. The process is vital because it transforms a collection of isolated semiconductor devices into a functional integrated circuit capable of performing complex operations.

The Metallization Process is not just about electrical connectivity; it also addresses challenges like resistivity, electromigration, and thermal stability. Metals with low resistivity ensure efficient electrical conduction, minimizing signal delay and power dissipation. Furthermore, metallization must resist electromigration, which is the migration of metal atoms due to high current densities, to ensure the long-term reliability of the device. Thermal stability is also critical, as the integrated circuit may experience a wide range of operating temperatures during its lifetime. Table 5.1 lists the most frequently used metals for the metallization process and some of their characteristic properties (Franssila, 2010).

Table 5.1. Properties of metals for the metallization process

Metal	Electrical Conductivity ($\Omega^{-1}\cdot m^{-1}$)	Melting Point (°C)	Thermal Conductivity (W/(m·K))	Resistivity ($\Omega\cdot m$)	Coefficient of Thermal Expansion (10^{-6}/°C)
Aluminum (Al)	3.8×10^7	660	237	2.65×10^{-8}	23
Copper (Cu)	5.9×10^7	1085	398	1.68×10^{-8}	16.6
Tungsten (W)	1.77×10^7	3422	174	5.65×10^{-8}	4.5
Titanium (Ti)	2.3×10^6	1668	21.9	4.2×10^{-7}	8.6
Nickel (Ni)	1.4×10^7	1453	90.9	6.99×10^{-8}	13.3

Advancements in metallization technology have been instrumental in the relentless pursuit of higher performance and functionality in microelectronics. As device dimensions shrink to nanoscale levels, the aspect ratio of vias and trenches becomes increasingly challenging. To overcome this, advanced deposition techniques, such as physical vapor deposition (PVD) and chemical vapor deposition (CVD), have been developed to achieve conformal and uniform metal layers.

The choice of metal in the metallization process also plays a significant role. While aluminum has historically been the preferred material (Hassanin et al. 2019), copper has emerged as a viable alternative due to its superior electrical conductivity. The transition from aluminum to copper metallization posed new challenges, such as copper diffusion into the silicon substrate, leading to the development of barrier layers to prevent these interactions.

6. DESIGN OF GRAPHENE-BASED NANOSTRUCTURED ISFET BIOSENSOR

6.1. Structure and Method of the proposed ISFET

The proposed graphene-based ISFET device is constructed in the SILVACO environment. Figures 6.1a and 6.1b illustrate the block diagram and the constructed structure in the simulation environment, respectively. As shown in the figures $GaAs$, Al_2O_3, graphene, and aluminum have been used as the substrate, sensitive layer, channel, and source/drain material, respectively. The gold region in Figure 1.b is used as a reference electrode. Some layer parameters are shown in Table 1, where the channel thickness is 10 nm, the length and thickness of the device are 600 nm and 800 nm, respectively.

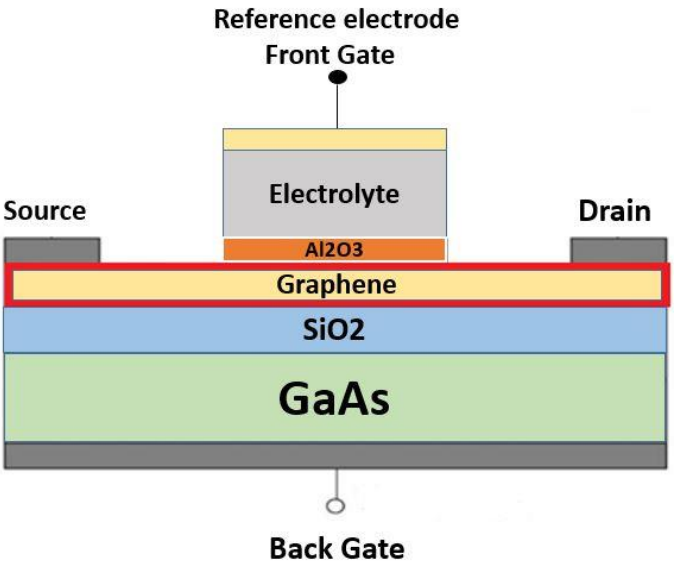

(a)

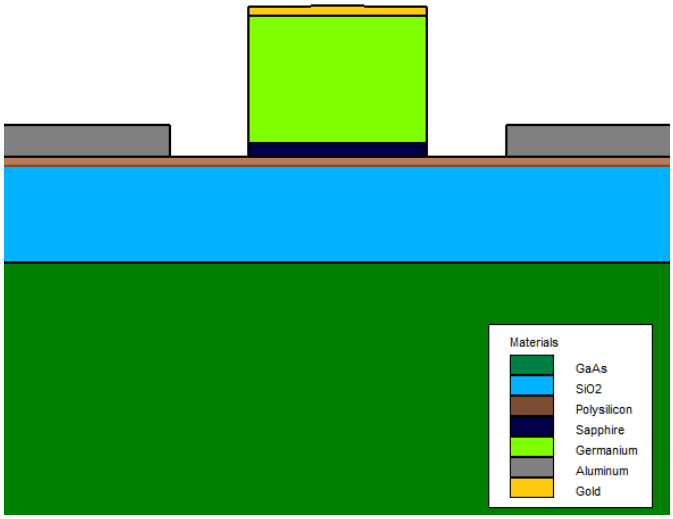

(b)

Figure 6.1. a) Block diagram and b) constructed structure of graphene based ISFET in Silvaco.

Table 6.1. Structural simulation parameters.

Parameters	**Graphene**	**GaAs**	**(Al_2O_3)**	**Fluid Gate**
permittivity	80	-	7.5	80
Thickness (nm)	10	400	10	200
Length (nm)	600	600	600	160
Affinity	-	-	-	3.9

In material science, the lattice constant refers to the distance between repeating units in a crystal lattice structure. It is a fundamental parameter that characterizes the arrangement of atoms or ions in a crystal lattice (Kajale et al. 2021). The lattice constant is typically represented by the symbol "*a*" and is measured in units of length, such as angstroms (Å) or picometers (pm).

In a crystal lattice, atoms or ions are arranged in a repeating pattern, forming a three-dimensional network of points called a lattice. The lattice constant defines the size and shape of the unit cell, which is the basic repeating unit of the crystal lattice. Each unit cell contains a certain number of atoms or ions, and the lattice constant determines its dimensions.

Different materials have different lattice constants, which depend on factors such as the crystal structure, type of bonding, and the types of atoms or ions present. For example, common crystal structures include cubic, tetragonal, orthorhombic, and hexagonal, each with its own characteristic lattice constant.

Designing a FET-based biosensor requires selecting materials with close lattice constants to each other. It is crucial for achieving a high-quality interface between the different layers of the device(M. Wu, Alivov, and Morkoç 2008). Table 6.2 shows the lattice constant of the materials used in constructing the device.

Table 6.2. Structure materials and their lattice constants

	GaAs	***SiO_2***	***Graphene***	***Al_2O_3***	***Germanium***	***Gold***
Lattice Constant Å	*5.65*	*5.31*	*5.43*	*4.81*	*5.66*	*4.08*

Since the graphene material and target electrolyte is undefined in SILVACO TCAD, software tools cannot simulate graphene. Instead, polysilicon and germanium layers can mimic them by changing their properties, such as bandgap, the density of states (DOS), mobility, affinity, and permittivity. Table 6.3 shows the properties and parameters of deposited polysilicon layer.

Transport equations for the holes-electrons in a semiconductor material and the cations-anions in an equilibrium electrolyte solution are similar (Bandiziol et al. 2015). Therefore, a monovalent electrolyte, with a bandgap of 1 eV and a dielectric constant equal to that of water, can be represented as a semiconductor with the density of states given by Equation (6.1).

$$\begin{aligned} N_C = N_V = \;& 10^{-3} N_{av}(c_0 + c_{HB}) && pH \leq 7 \\ =\; & 10^{-3} N_{av}(c_0 + 10^{-14}/c_{HB}) && pH > 7 \end{aligned} \tag{6.1}$$

where, c_0 and c_{HB} are the molar salt ion and hydrogen concentration in mol/l in the solution, respectively. N_C and N_V are expressed in cm^{-3}. N_C and N_V are $6.625310\, cm^{-3}$, while N_{av} is Avogadro's number. The bulk electrolyte can be defined as a region with constant potential and zero net electrolyte charge since the total concentrations of positive (p) and negative (n) ions are equal. Figure 6.2 illustrates the relationship between the density of states and different pH values (Dinar et al. 2019b).

$$\begin{aligned} n &\cong N_C e^{-\frac{E_C - E_f}{kT}} \\ p &\cong N_v e^{-\frac{E_f - E_v}{kT}} \end{aligned} \tag{6.2}$$

where, k is the Boltzmann constant, T is the temperature. E_V, E_C and E_f are the upper energy level of the valance band, lower energy level of the conduction band, and the Fermi energy level, respectively.

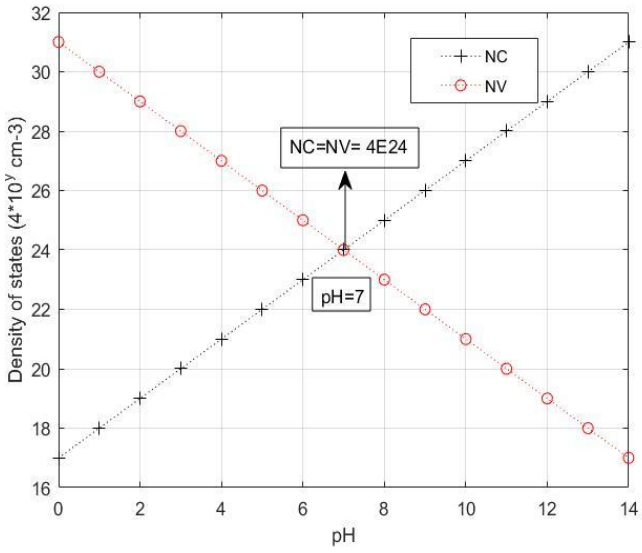

Figure 6.2. Density of states N_C and N_V versus pH values.

Table 6.3. Properties of deposited polysilicon and germanium layers

	Energy gap	**DOS** Valence band	**DOS** Conduction band	**Permittivity**	**Electron mobility**	**Hole mobility**	**Affinity**
Polysilicon	0.1	$377x10^{15}$	$377x10^{15}$	80	300	30	-
Germanium	1	$4x10^{21}$	$4x10^{27}$	80	-	-	3.9

6.2. Microfabrication of the proposed ISFET

The structural design and microfabrication of the nanostructured Graphene ISFET in the proposed electrode were simulated using the TCAD Silvaco electronic design automation and technology computer-aided design tool (Ahmed Harb et al. 2023). The device is simulated by a two-dimensional numerical semiconductor processing simulator. The microfabrication process flow chart is shown in Figure 6.3, and the methodology is described below. The Silvaco code containing the whole microfabrication process is provided in Appendix A.

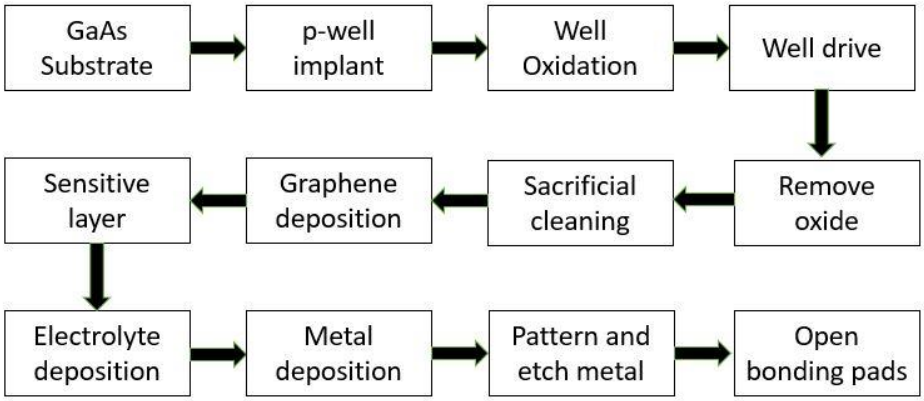

Figure 6.3. ISFET Flow chart of ISFET microfabrication

Gallium Arsenide (GaAs) wafer in the <100> orientation has been chosen as a substrate material in the development of n-channel ISFET. The wafer was doped with boron at a concentration of $10x10^{15}$ cm^{-2}, as shown in Figure 6.4.

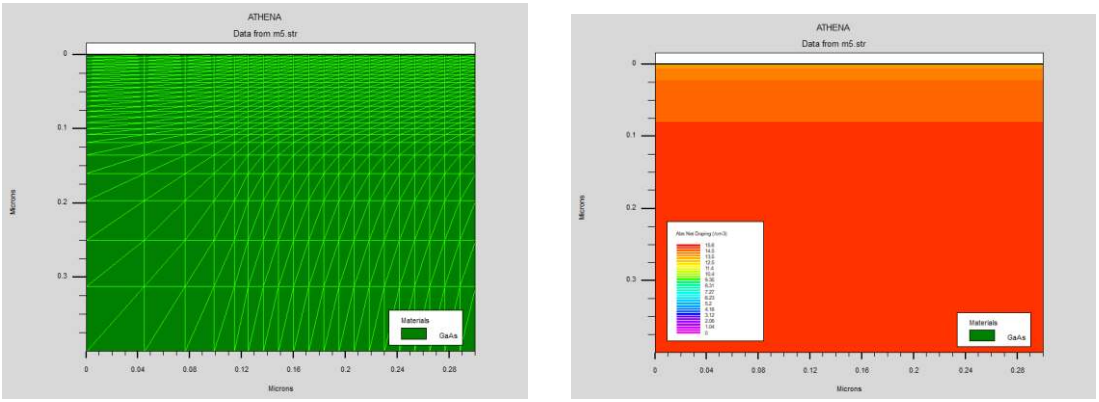

Figure 6.4. Substrate structure and doping concentration

The next step was well oxidation, depositing 0.15 um of the doped oxide layer over the substrate. The characteristics of ISFETs are significantly influenced by the gate oxide thickness, which is represented as a blue layer on the substrate structure in Figure 6.5.

Boron atoms were implanted at a dose of $10x10^{14}$ cm^{-2} to adjust the threshold voltage of the n-channel ISFET device. A higher dose of boron atoms implanted leads to an increase in the ISFET threshold voltage.

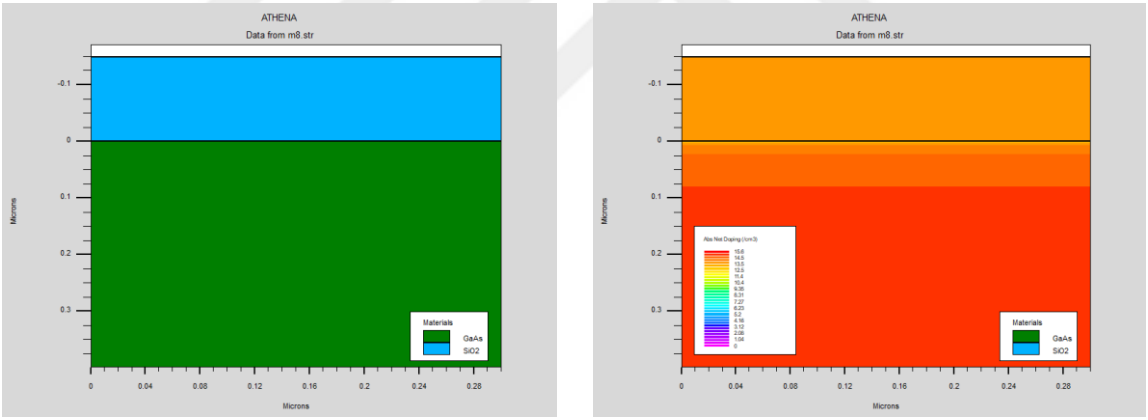

Figure 6.5. Structure and doping concentration after well oxidation

The next step in the microfabrication is the graphene layer deposition to create the channel of the ISFET. It is a similar step to previously explained oxide deposition. The polysilicon gate layer was deposited with a thickness of 10 nm. The two-dimensional structure of the graphene channel is shown in Figure 6.6.

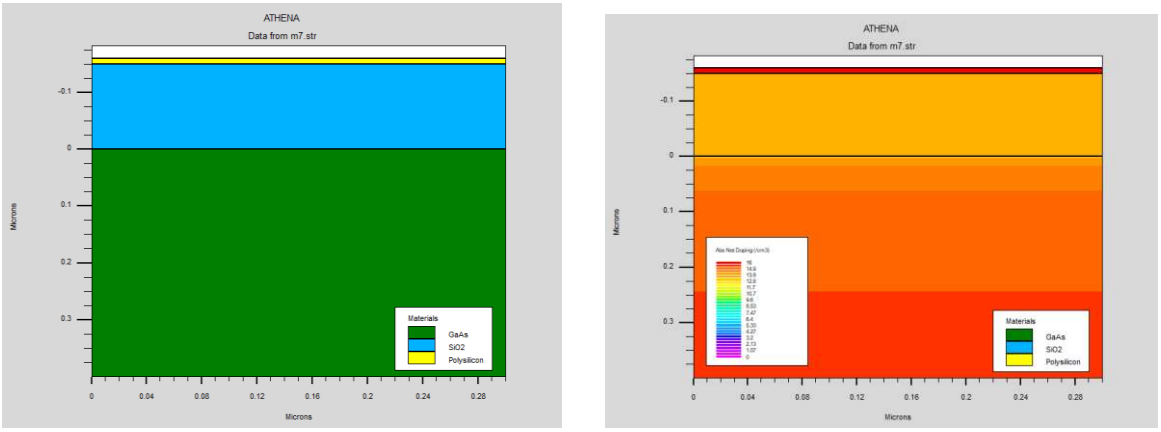

Figure 6.6. Structure and doping concentration after graphene deposition

Over the channel region, a thin, sensitive layer of Al2O3 is formed as a top gate by the deposition process, and then etched anisotropically, as shown in Figure 6.7.

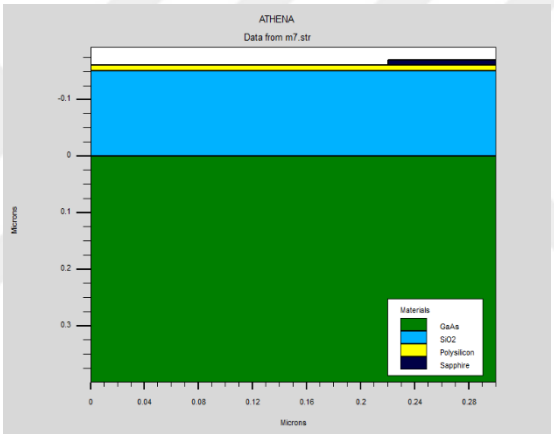

Figure 6.7. ISFET structure after sensitive layer deposition

Germanium, with specific parameters, is deposited then over the sensitive layer to simulate the target electrolyte, as described in section 6.1. Figure 6.8 illustrates the design after the germanium deposition process.

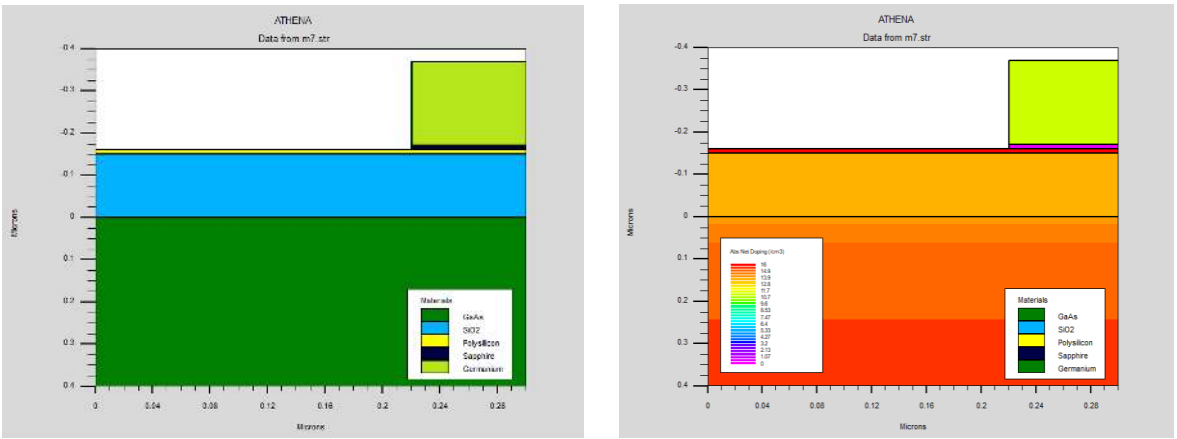

Figure 6.8. ISFET structure and doping concentration after electrolyte deposition

Metallization is the last process. Aluminum and gold are deposited for the source, drain, and gate terminals. Figure 6.9 illustrates the final structure of the proposed device after metallization.

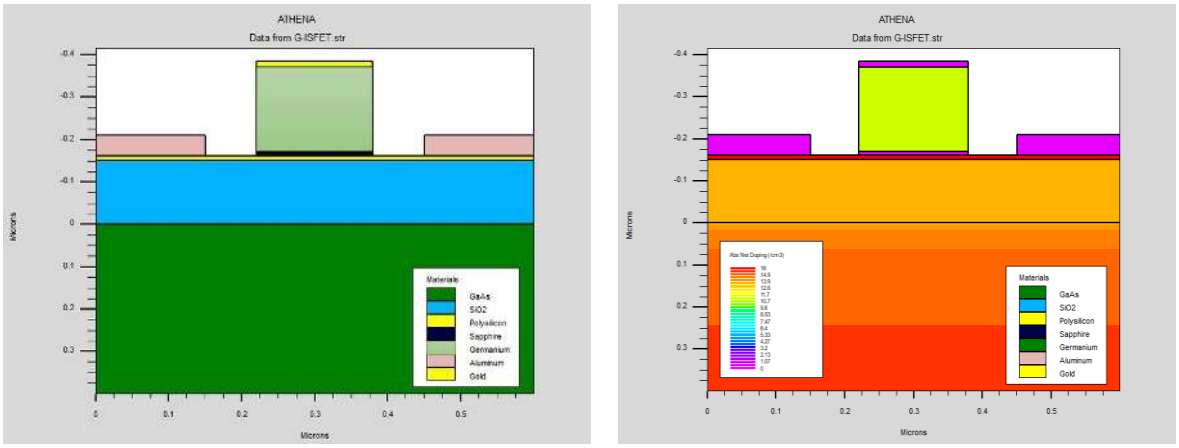

Figure 6.9. Final ISFET structure and doping concentration after metallization.

6.3. Extracting parameters of the proposed ISFET

At the end of the microfabrication process of the proposed ISFET, some parameters of the designed device are extracted to use in the Cadence Virtuoso environment in order to conduct other tests and experiments such as stability, linearity, stability, temperature-dependency, and the others. Table 6.4 shows the extracted device parameters.

Table 6.4. Extracted parameters and used ATHENA code

Parameter	Value
Material thickness (Substrate)	0.4 um
Sheet resistance	0.5E-6 ohm
Bulk Fermi potential	0.5 V
Junction depth	300E-3 um
Gate oxide capacitance	2.0E-3 F

6.4. Simulation Results

6.4.1. Electrical Characteristics

A constant voltage is applied to the gate terminal (from 0 to 3 V). In this case, the drain current is increased as the drain-source voltage increases. The characteristic output curve of the proposed device is given in Figure 6.10a for various gate voltages (0-3V) with 1V step size and drain-source voltages in the range of 0-2V with 10mV step size. It is demonstrated that large gate voltages yield large drain currents. This is consistent with the saturation condition of the drain current in a classical MOSFET. The drain current can reach 0.33 mA at $V_{GS} = 3V$.

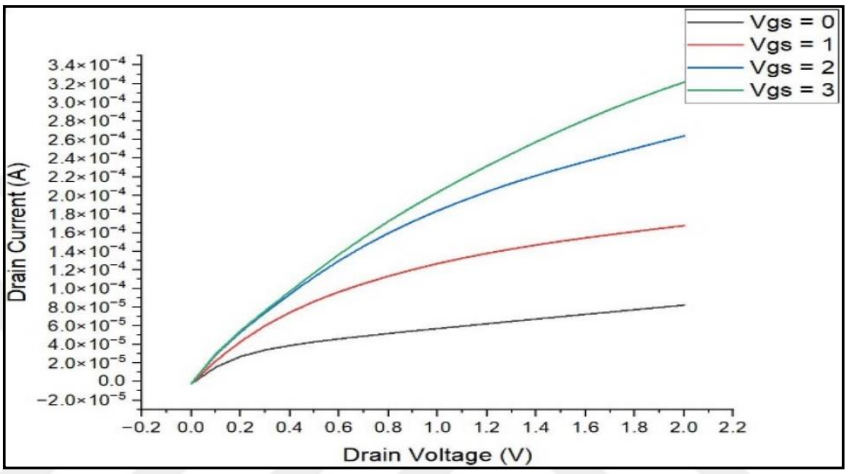

(a)

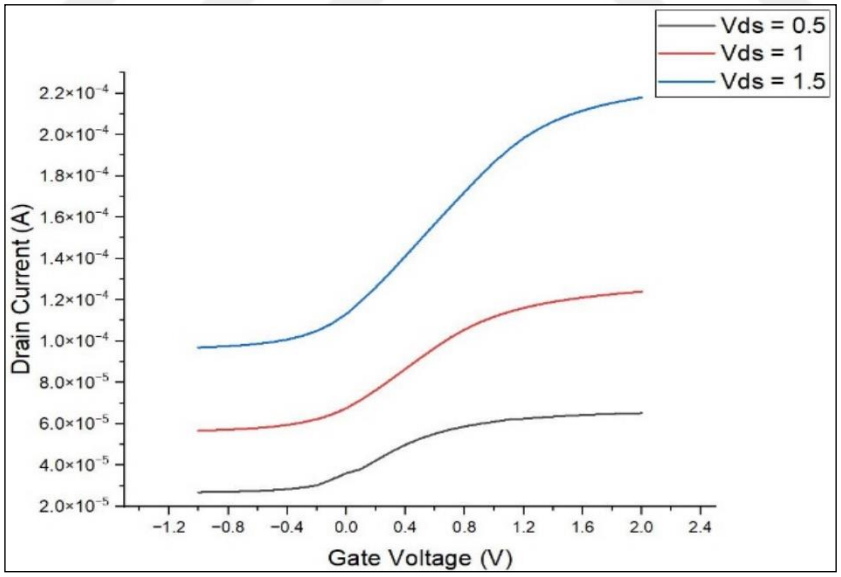

(b)

Figure 6.10. a) $I_D - V_D$ and b) $I_D - V_G$curves of the proposed device.

Figure 6.10b illustrates the transfer characteristics of the device, demonstrating the gate voltage's capability to control the drain current. The transfer characteristics curve is obtained by setting the source-drain voltage to 0.5V, 1V, and 1.5V, respectively, and sweeping the gate voltage from 1 to 2V. The threshold voltage (V_{th}) is acquired as 0.5V.

6.4.2. Sensitivity Analysis

The proposed device is analyzed regarding several sensitive layers. ISFETs with (Al_2O_3) sensitive layer provides better sensitivity than those of (SiO_2) and (Si_3N_4). The sensitivity of the front-gate scanning method for the proposed ISFET with aluminum oxide sensing material is 59.5 mV/pH, which is slightly higher than the Nernst limit (59 mV/pH). Table 6.5 also gives the sensitivity simulation results for different sensing layers.

Table 6.5. Sensitivity of front-gate scanning for different sensing films.

Sensing Film	Sensitivity (mV/pH)
Aluminum Oxide (Al2O3)	59.5
Silicon Nitride (Si3N4)	56.8
Silicon Dioxide (SiO2)	56.1

pH level fluctuations in the target solution change the (Dinar et al. 2019a)carrier concentration in the channel, which also alters the p-n junction characteristics and the drain current amplitude. On the other hand, different V_{th} values correspond to different pH values (Wang and Tang 2021). Therefore, the device sensitivity can be determined as in Equation (6.3) by detecting the change in threshold voltages.

$$sensitivity = \frac{V_{th}(pH_2) - V_{th}(pH_1)}{pH_2 - pH_1} \tag{6.3}$$

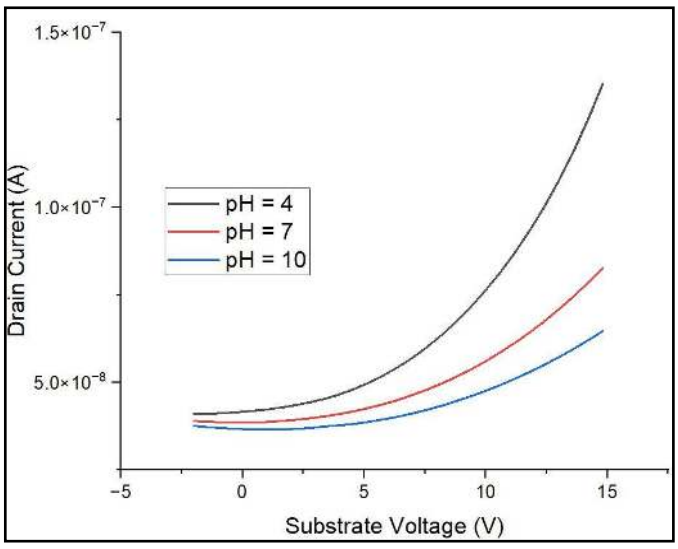

Figure 6.11. ISFET transfer characteristics with different pH value

7. READOUT CIRCUIT: DESIGN, MODELLING AND ANALYSIS

Since the output signal from the ISFET is weak, signal amplification is required. This can be done by using the readout circuit. There are various readout circuit types that can be utilized for amplification. The ISFET and readout circuit can be integrated to create an ISFET sensor.

7.1. Cadence Virtuoso: Overview

Cadence Virtuoso is a leading Electronic Design Automation (EDA) tool suite developed by Cadence Design Systems. It serves as a comprehensive environment for designing and verifying complex analog, digital, and mixed-signal integrated circuits (ICs). With Virtuoso, engineers can seamlessly create, simulate, and analyze various aspects of their IC designs. The suite includes a powerful Schematic Editor for creating and modifying circuit schematics, enabling efficient hierarchical design management. The Layout Editor provides a flexible platform for designing the physical layout of ICs, allowing precise placement and shape definition of components. Virtuoso seamlessly integrates with simulation tools like Spectre and Virtuoso Simulation, enabling comprehensive circuit-level simulations for functional and performance verification. Additionally, Virtuoso incorporates Design Rule Checking (DRC) capabilities, ensuring compliance with manufacturing rules and constraints. The suite also offers extraction and verification tools to account for parasitic effects and facilitate post-layout simulations. Overall, Cadence Virtuoso empowers designers to streamline their IC design workflows and achieve accurate and reliable results for successful chip fabrication.

7.2. Design and development of ISFET and electrolyte models

As Cadence virtuoso initially does not have any instance for ISFET and electrolyte, Custom models have been developed by Verilog-A language to provide the intended instances of our readout circuit.

7.2.1. Graphene ISFET model

Through the years, modeling and simulation have proven to be invaluable in the advancement of transistor technologies by acting as crucial tools for establishing the relationships between device performance, design parameters, and fabrication techniques. The primary work involved in modeling a GFET was not published until 2010 (Mappes, 2022), despite the fact that the first successful benchtop demonstration of a GFET was reported in 2004. This work served to provide a charge carrier concentration model as well as a mathematical model for drain current.

A Verilog-A code, described in Appendix B, has been developed to design the Gr-ISFET instance illustrated in Figure 7.1, to be used then in the Cadence Virtuoso environment. The model's parameters and characteristics are editable. Therefore, the extracted parameters from TCAD Silvaco design can be imported easily as shown in Table 7.1.

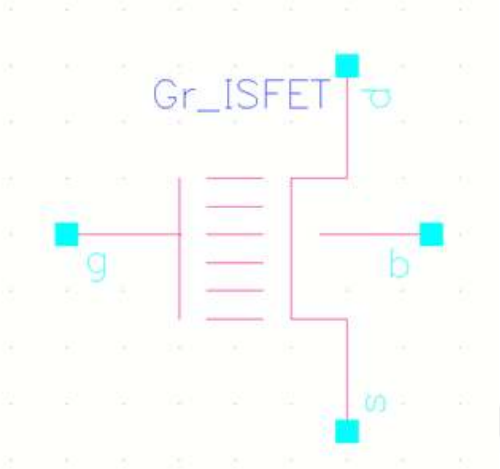

Figure 7.1. Gr-ISFET instance in Cadence virtuoso

Table 7.1. The editable parameters and properties of the developed Gr-ISFET model

Symbol	Parameter	Value
L	Channel length	0.4 µm
W	Channel width	0.5E-6 ohm
Cox	Gate oxide capacitance	0.5 V
XJ	Junction depth	300E-3 µm
VTO	Gate oxide capacitance	2.0E-3 F
GAMMA	Body effect parameter	0.7
PHI	Bulk Fermi potential	0.5 V
E0	Mobility reduction coefficient	1.0E8 V/m

The primary objective of the model is to support the design of low-power analog ICs by providing a single analytical expression that is precise in all modes of device operation, including the weak and moderate inversion regimes.

7.2.2. Electrolyte model

The concentration of hydronium ions (H+) in a solution is measured by the potential of hydrogen (pH), which is a crucial indicator for many chemical and biological systems. The electrolyte model for the FET pH sensor demonstrates the working principle of a field-effect transistor (FET) with the target solution in order to monitor its pH. The model has been developed by Verilog-A, as described in Appendix C, to be used with the Gr-ISFET model in the Cadence

Virtuoso environment, see Figure 7.2a. it is adaptable and can be applied to various FET pH-sensor classes.

The pH affects the potential across the electrolyte, which is the difference between the fluid gate voltage (V_{fg}) and effective gate voltage (V_{geff}), as shown in Figure 7.2b and Equation 7.1. As a result, a pH-dependent voltage source (ψ_0) can be used to record the sensor's pH dependence. pH can be modeled as an external voltage source (V_{pH}) for circuit simulation (Dak and Alam 2014). Although pH is not a voltage source physically in the same way that a battery is, the compact model can view pH's impact on transistor I-V characteristics as a voltage source. The circuit simulator's transient and small signal analysis with respect to pH is made possible by the definition of pH as a voltage source.

$$Vgeff = Vfg - \psi 0 \quad (7.1)$$

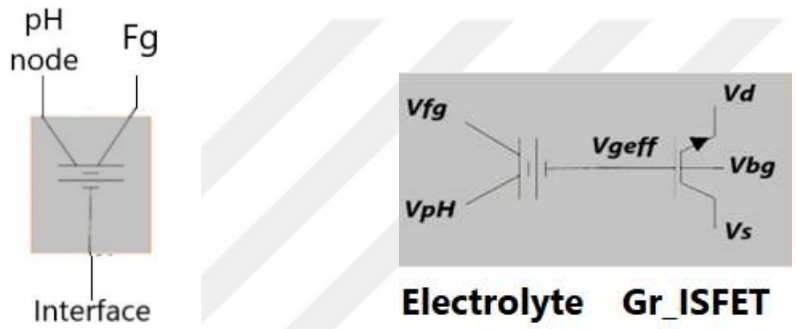

(a) (b)

Figure 7.2. (a) Electrolyte model (b) Representation of a pH sensor

Table 7.2. Parameters and physical quantities.

Node	Description
pHnode	$-\log_{10}[H+]$
Fg	Fluid gate voltage
Interface	Effective gate voltage (Vgeff)

Table 7.3 shows the editable parameters and characteristics of the electrolyte model, these parameters can be edited easily from the properties window of the electrolyte instance in Cadence Virtuoso software.

Table 7.3. Parameters used in the electrolyte model and their physical meaning (Dak and Alam, 2014).

Symbol	Verilog-A Symbol	Description	Default value	Unit
pKa	*pKa*	$-\log_{10}[\mathrm{Ka}]$ where $\mathrm{Ka} = \frac{[\mathrm{AOH}][\mathrm{Hs}+]}{[\mathrm{AOH_2}+]}$ is the acid dissociation constant.	-2	-
pKb	*pKb*	$-\log_{10}[\mathrm{Kb}]$ where $\mathrm{Kb} = \frac{[\mathrm{AO}-][\mathrm{Hs}+]}{[\mathrm{AOH}]}$ is the base dissociation constant.	-6	-
Cstern	*Cstern*	Capacitance of the stern layer	0.2	F/m2
-	*sternmod*	sternmod=0 for using GC model, sternmod=1 for using GCS model	1	-
NOH	*NOH*	Density of the surface groups	5×10^{14}	cm−2
i0	*i0*	Ionic concentration of the buffer solution	0.1	Molar

Effective gate potential (V_{geff}) of the transistor is determined using the following set of equations (Dak and Alam 2014).

$$V_{geff} \equiv V_{fg} - \psi_0 \tag{7.2}$$

$$\psi_0 \equiv -\log_e 10 \times v_t \times \alpha \times (pH - pH_{pzc}) \tag{7.3}$$

where, pH_{pzc} is pH value at which the surface charge becomes zero.

$$pH_{pzc} = \mathrm{pKa} + \mathrm{pK_b} \tag{7.4}$$

$$\alpha \equiv \frac{\beta}{1+\beta} \tag{7.5}$$

with β defined as:

$$\beta = q\, N_{OH} \times \frac{\delta}{Ceq \times \mathrm{Vt}} \tag{7.6}$$

with,

$$C_{\mathrm{eq}} = \frac{Cdl \times Cstern}{Cdl + Cstern} \tag{7.7}$$

where, Cdl is the double layer capacitance at zero surface potential.

7.3. Readout circuit: MOSFET differential amplifier

The readout circuit is a crucial part of the biosensor system. This circuit design plays an important role in converting the insignificant variations in the output of the ion-sensitive field-effect transistor (ISFET) biosensor into understandable and quantifiable signals. The readout circuit, illustrated in Figure 7.3, uses the Gr_ISFET and Electrolyte models, which have been developed previously, as discussed in the section 7.2. The circuit has two parts; the first includes the predeveloped models in addition to an enhancement load (MOSFET resistor) connected to the drain of the Gr_ISFET to modify the differential amplifier input voltage and make sure that it less than the maximum value. The other part of the circuit includes the differential amplifier, voltage comparator and output load. The 90 nm Generic Process Design Kit (gpdk090) library has been used to develop the circuit in Cadence Virtuoso environment.

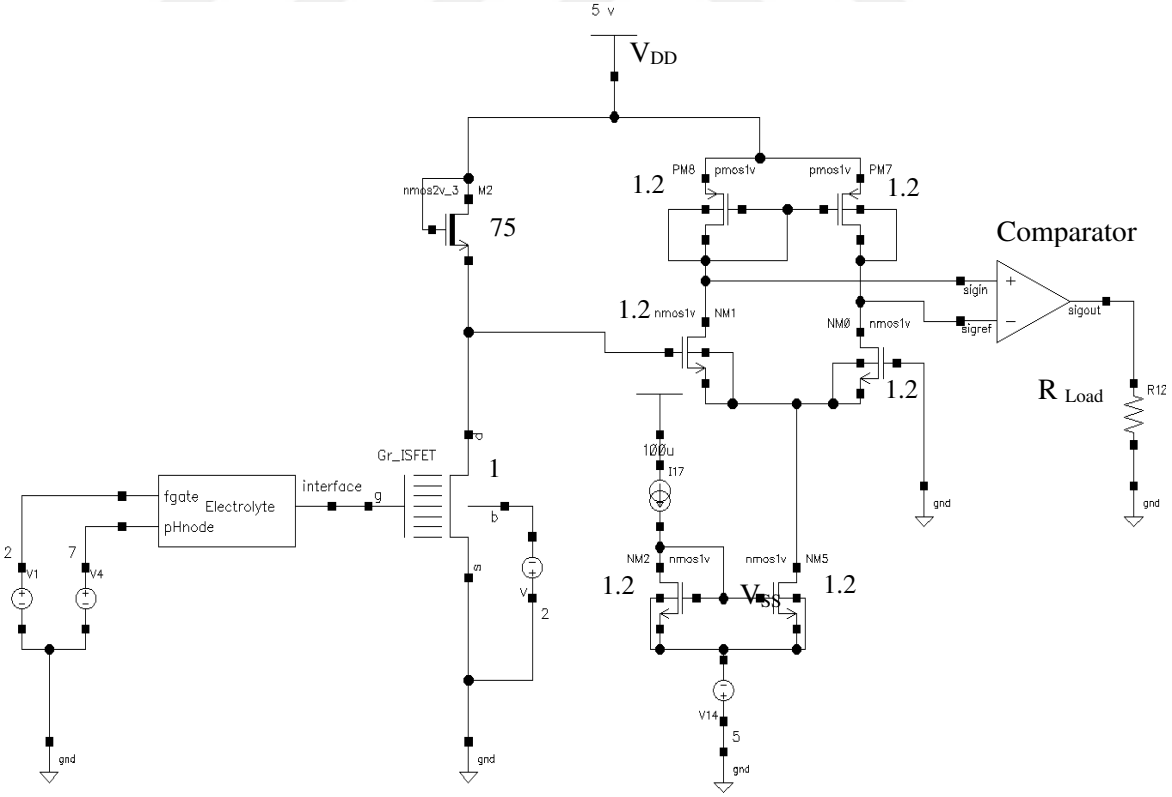

Figure 7.3. Proposed ISFET readout circuit

Figure 7.4 shows a basic MOSFET differential amplifier circuit. In this circuit, $M1$ and $M2$ are two identical transistors and the source terminals of the transistors are connected to each other. The current of both transistors is determined by the current source IQ, which connected to V_{SS}.

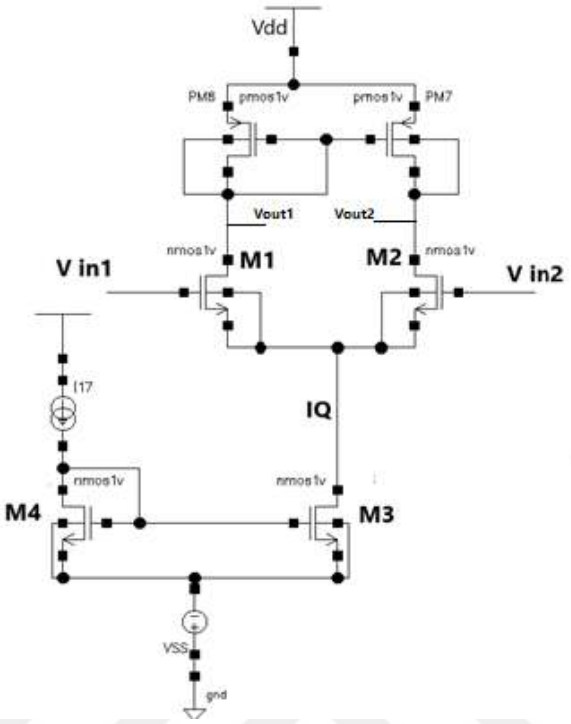

Figure 7.4. Basic MOSFET differential amplifier circuit

In differential amplifiers with MOSFETs, $M1$ and $M2$ transistors are designed to remain in saturation. Since the transistors are equivalent, when the input voltages are zero or the same, the drain currents of both must be equal, and the sum of these currents IQ must be equal to the current of the current source (İstanbullu and Avcı, 2020). In this case:

$$I_Q = I_{D1} + I_{D2} \tag{7.8}$$

$$ID1 = ID2 = ID = \frac{IQ}{2} \tag{7.9}$$

$$V_{Out1} = V_{Out2} = V_{DD} - RD(I_Q/2) \tag{7.10}$$

So, the output voltage of the circuit is:

$$V_{OutDC} = V_{Out2} - V_{Out1} = 0 \tag{7.11}$$

On the other hand, when V_{in1} is more than V_{in2}, the voltage drop in the left-hand sided RD will increase as I_{D1} will be more than I_{D2}. As a result, V_{Out1} will decrease.

The minimum and maximum values of Vin1 and Vin2 are given by Equation 7.12 and 7.13:

$$V_{in(max)} \leq V_{DD} - \frac{I_Q}{2} RD + V_{TH} \tag{7.12}$$

$$V_{in(min)} = V_{DD} - V_S + V_{GS} \tag{7.13}$$

where, VDD is the drain voltage, RD is the drain resistor, VTH is the threshold voltage, VS is the source voltage and VGS is the gate-source voltage. The drain current I_D and the gate-source voltage V_{GS} are given by Equation 7.14 and Equation 7.15 respectively:

$$ID = \frac{\mu_n Cox}{2}\left(\frac{W}{L}\right)(V_{GS} - V_{TH}) \tag{7.14}$$

$$V_{GS} = \sqrt{\frac{IQ}{\mu_n Cox\left(\frac{W}{L}\right)}} + V_{TH} \tag{7.15}$$

where, the μ_n is electron mobility, C_{ox} is the CMOS oxide capacitance per unit area and W/L is width-to-length ratio of the channel.

In this work, the parameters and specifications of the differential amplifier, illustrated in Figure 7.4, and chosen technology are listed in Table 7.4.

Table 7.4. Design specifications of the differential amplifier

Device technology	90 nm gpdk090
$V_{in(max)}$	250 mV
$V_{in(min)}$	5 mV
V_{DD}	5 V
V_{SS}	-5 V
IQ	186 µA
Gate-source Voltage (V_{GS})	870 mV
VTH	1 V

7.4. Simulation Results

This section covers the in-depth evaluation and interpretation of the results from the meticulous simulations carried out for this study. Sensitivity, linearity, stability, and temperature-dependency are included in the simulations and all of which are crucial for determining the effectiveness and dependability of the suggested system. This chapter represents a significant turning point in our thesis because it not only establishes the validity of the theoretical framework but also provides a foundation from which to infer important conclusions and offer suggestions for further development.

7.4.1. Sensitivity Analysis

In the simulation, the drain to source and front-gate (V_{ref}) voltages are adjusted to 5V and 2V, respectively. The back-gate voltage is swept after that. The sensitivity of the device is tested with various pH values (4, 7, and 10), as shown in Figure 7.4, to confirm the accuracy of the proposed model. It is obvious that increasing pH raises the threshold voltage and shifts the overall trend to the right. The calculated sensitivity of the device in this analysis reached roughly 1000 mV/pH, which is better than the studies in the literature. As mentioned in Equation 6.3, the sensitivity can be calculated as follows considering pH1 is 7 and pH2 equal 10:

$$sensitivity = \frac{V_{th}(pH_2) - V_{th}(pH_1)}{pH_2 - pH_1} = \frac{6-3.1}{10-7} \approx 1000\ mV/pH \tag{7.16}$$

These results greatly converged with the sensitivity analysis results, which were derived from ATHENA in TCAD Silvaco as discussed previously in chapter 6.4.2. The proposed graphene-based device presents higher sensitivity score compared to the literature (see Table 3.1).

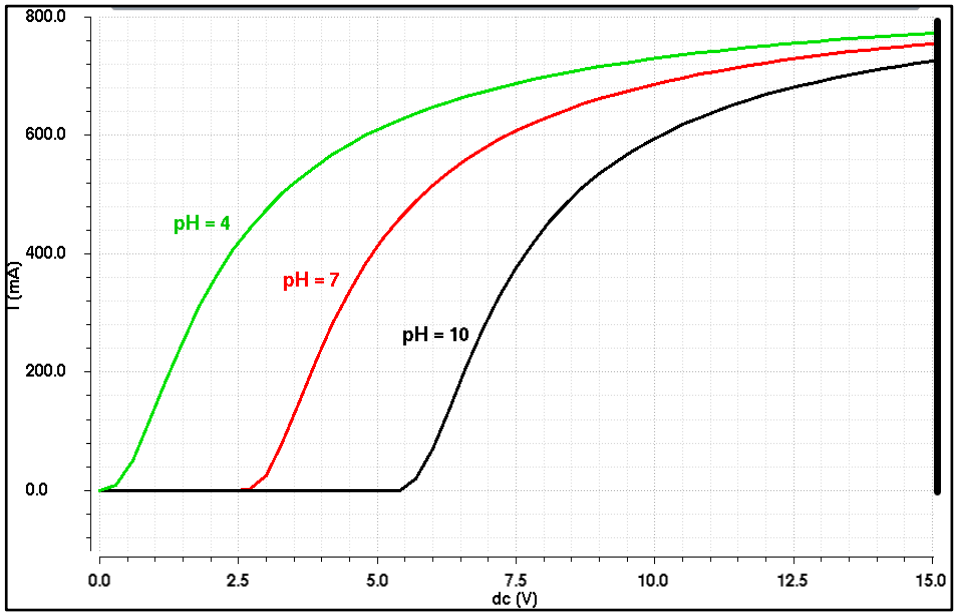

Figure 7.5. Transfer characteristics of the proposed device with pH values 4,7 and 10

7.4.2. Linearity test

After analyzing the corresponding output voltage regarding the pH values, valuable insights have been gained into the sensor's ability to maintain a linear relationship between its electrical response and the pH changes. A highly linear response is essential for accurate and reliable pH measurements, making the linearity test an indispensable aspect of this study.

The pH value of the electrolyte has swept from 1 to 14 and the output current has been recorded. Figure 7.5 shows the results, which indicate the impact of the proposed readout circuit on the linearity of the device.

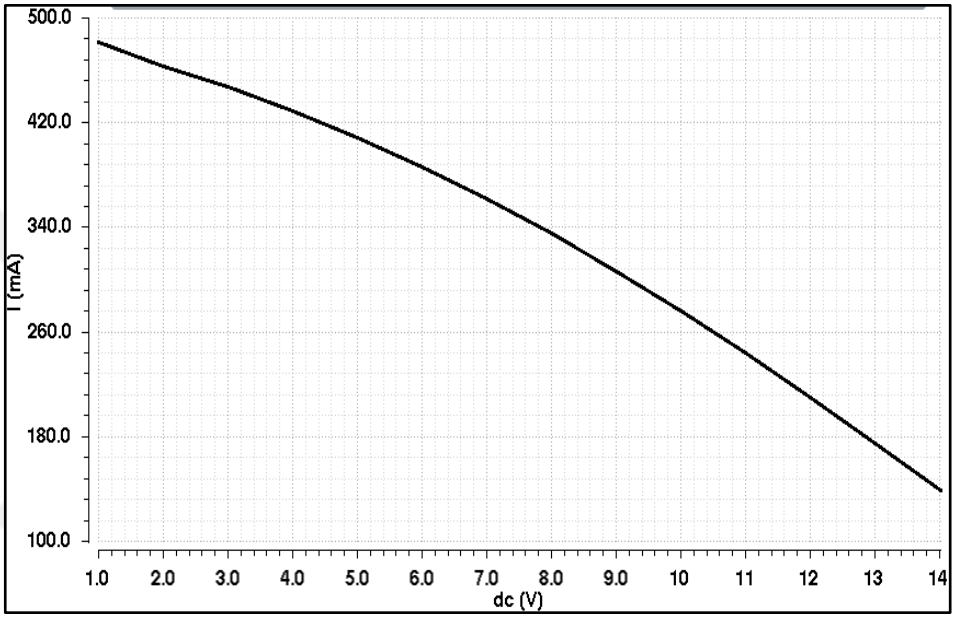

Figure 7.6. pH values versus the output current of the proposed device

7.4.3. Stability analysis

In this analysis, the ISFET biosensor is subjected to continuous pH measurements over an extended period, during which its response is monitored and recorded. The stability test allows us to ascertain the sensor's ability to maintain consistent and accurate pH readings over time, reflecting its resilience to environmental and operational fluctuations.

Following the initial period of ISFET stabilization, the drift rates were assessed as a linear change in V_{GS} per time unit. After applying the proposed circuit, long-term drift is reduced considerably. The ISFET was tested for 1000 seconds in a standard buffer solution with a pH of 4,7 and 10 at a constant temperature of 25 °C and the output voltage has been recorded. The time response of the ISFET is shown in Figure 7.6.

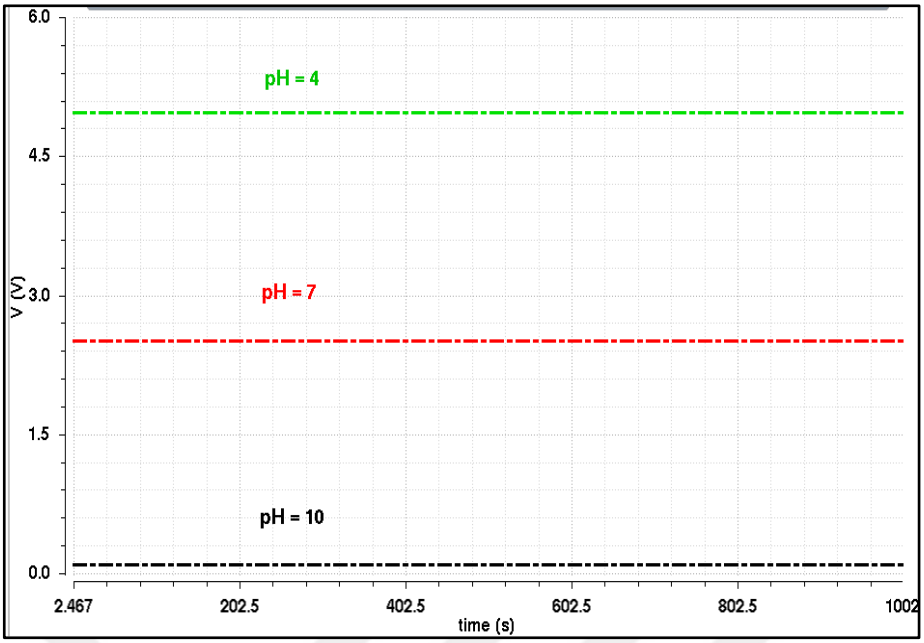

Figure 7.7. Stability analysis of the proposed device with pH value 4,7 and 10

7.4.4. Temperature-dependency test

In this experiment, the ISFET was operating with an electrolyte solution at pH 4, 7 and 10 with temperature swept from 0 to 50 ◦C. Figure 7.7 illustrates the V_{out} versus temperature results, which indicates that the temperature-dependency of the ISFET with its readout circuit has been reduced.

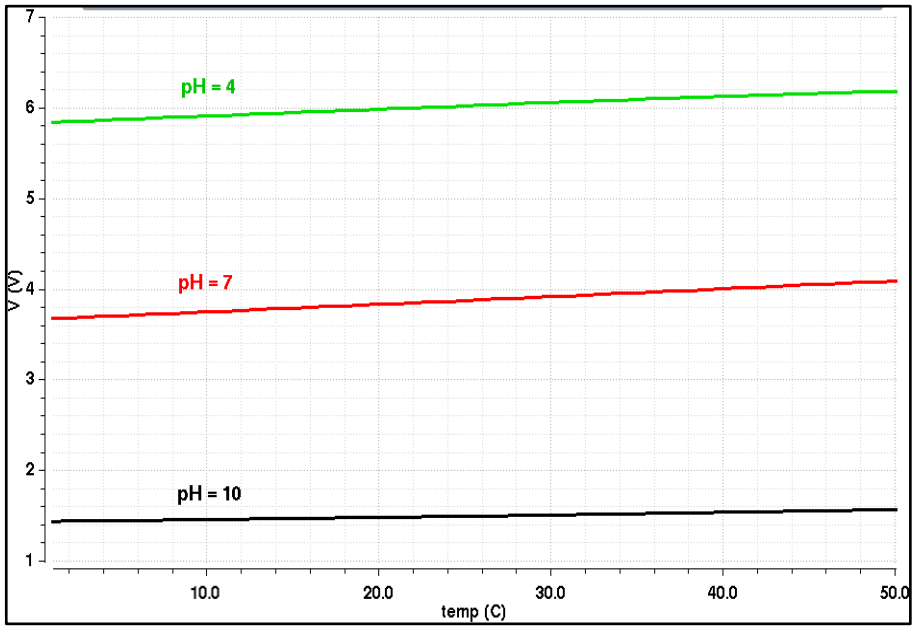

Figure 7.8. Temperature-dependency with pH value 4,7 and

8. CONCLUSIONS

This thesis has presented a comprehensive study on the design and simulation of a graphene-based dual-gate nanostructured ISFET biosensor. The primary objective was to overcome the limitations of traditional ISFET biosensors by harnessing the exceptional properties of graphene and integrating it into a sophisticated dual-gate architecture. The research journey unfolded across eight chapters, each contributing valuable insights to the development of advanced biosensor technology.

First, we have provided an introduction to the research, highlighting the significance of biosensors and the motivation behind exploring graphene as a sensing material. The specific objectives were outlined, setting the direction for the subsequent chapters. The preliminary work established the foundation by reviewing existing research related to ISFET biosensors and graphene. This literature review served to identify research gaps and understand the challenges faced by conventional ISFET devices.

After that, ISFET biosensors have been discussed generally. It explored the operational principles and applications of ISFET biosensors, discussing the limitations and emphasizing the need for innovative solutions. Moreover, the study focused on graphene, showcasing its exceptional properties that make it an attractive candidate for sensitive and selective biosensing. After that, the microfabrication processes have been discussed, covering diffusion, ion implantation, lithography, etching, and metallization processes involved in integrating graphene into the ISFET biosensor. This understanding was essential for ensuring the manufacturability and reliability of the proposed device.

The design of the graphene-based dual-gate nanostructured ISFET biosensor has been presented then, detailing its structure, fabrication method, and TCAD Silvaco simulation results. The successful integration of graphene into the dual-gate architecture demonstrated enhanced sensitivity and selectivity for biomolecular detection. During the design, modeling, and analysis of the readout circuit has been discussed in chapter 7, a critical component responsible for translating sensor signals into meaningful data. Cadence Virtuoso simulations provided valuable insights into the circuit's performance, including sensitivity analysis, linearity testing, stability analysis, and temperature-dependency evaluation.

This thesis analyzes the effect of the graphene layer, as a channel material, on the performance of the ISFET device. The device is tested using the electrolyte model implemented in the Silvaco environment. The acquired characteristic curves are also physically examined. The effects of the back gate, channel material, and sensitive layer on device performance are considered by assessing the electrical characteristics, threshold voltage, and drain current. The proposed device is constructed using GaAs as a substrate, graphene as the channel material, and Al_2O_3 (sapphire) as the sensitive film. Graphene-based ISFETs provide better sensitivity than conventional types, and the threshold voltage shows variations upon changing the electrolyte pH level. The channel thickness

in the proposed structure is 10nm. Consequently, the proposed ISFET device has a pH detection sensitivity of $1066\ mV/pH$.

The dual-gate graphene-based nanostructured ISFET biosensor that has been proposed throughout this study has shown great promise for sophisticated biosensing applications. The biosensor overcame the limitations of conventional ISFET devices by utilizing the exceptional characteristics of graphene and implementing an effective dual-gate architecture.

By successfully designing and simulating the graphene-based biosensor and illustrating its use in biotechnology, environmental monitoring, and medical diagnostics, this thesis makes contributions. Using graphene as a channel material and a dual-gate nanostructure as proposed provides a novel approach to enhance the performance of ISFET biosensors.

As we conclude this study, it is essential to acknowledge that there are still opportunities for further research. Experimental validation of the graphene-based biosensor's performance and characterization in real-world conditions will be crucial for its practical implementation. Further optimization of the biosensor's specificity for detecting specific biomolecules and the investigation of miniaturization and integration into portable devices hold promise for point-of-care applications.

REFERENCES

A RF Graphene FET Large-Signal Compact Model Compatible with Circuit Simulators by Scott M . Trocchia B . S . in Computer Engineering , May 2011 , The George Washington University A Thesis Submitted to The Faculty of The School of Engineering and Applied .” 2012. (May 2011).

Al-ahdal, Abdulrahman Ghaleb I. 2012. “Floating Gate ISFET Chemical Inverters : For Semiconductor Based Biomedical Applications.” (July).

Bandiziol, Andrea et al. 2015. “A TCAD-Based Methodology to Model the Site-Binding Charge at ISFET/Electrolyte Interfaces.” *IEEE Transactions on Electron Devices* 62(10): 3379–86.

Baylay, Murat. 2010. “Ion-Sensitive Field Effect Transistor (ISFET) for MEMS Multisensory Chips at RIT Acknowledgment.” (October 2010): 1–67.

Bergveld, P. 2003. “ISFET, Theory and Practice.” In *IEEE Sensor Conference*, Toronto, 1–26.

Cacho-Soblechero, Miguel et al. 2020. “A Dual-Sensing Thermo-Chemical ISFET Array for DNA-Based Diagnostics.” *IEEE Transactions on Biomedical Circuits and Systems* 14(3): 477–89.

Cao, Shengli et al. 2022. “ISFET-based Sensors for (Bio)Chemical Applications: A Review.” *Electrochemical Science Advances* (November 2021): 1–25.

Chang, Yuh-Hwa et al. 2011. “Highly Sensitive PH Sensing Using an Indium Nitride Ion-Sensitive Field-Effect Transistor.” *IEEE Sensors Journal* 11(5): 1157–61.

Chao, Lemeng et al. 2020. “Applications of Field Effect Transistor Biosensors Integrated in Microfluidic Chips.” *Nanoscience and Nanotechnology Letters* 12(4): 427–45.

Choksi, Neel et al. 2017a. “Modeling and Simulation of Ion-Sensitive Field-Effect Transistor Using TCAD Methodology.” In *2017 1st International Conference on Electronics, Materials Engineering and Nano-Technology (IEMENTech)*, , 1–4.

Dak, Piyush, and Muhammad Ashraful Alam. 2014. “FET PH Sensor Model.” *nanoHUB*: 1–16. https://nanohub.org/publications/11/1.

Dinar, Ahmed M. et al. 2019a. “Modeling and Simulation of Electrolyte PH Change in Conventional ISFET Using Commercial Silvaco TCAD.” *IOP Conference Series: Materials Science and Engineering* 518(4).

Elyasi, Ali, Majid Fouladian, and Shahriar Jamasb. 2018. “Counteracting Threshold-Voltage Drift in Ion-Selective Field Effect Transistors (ISFETs) Using Threshold-Setting Ion Implantation.” *IEEE Journal of the Electron Devices Society* 6(September): 747–54.

Erismis, Mehmet Akif. 2013. “A Review On Variable MEMS Mirrors For Photo-Lithographic Masks.” *Academic Platform Journal of Engineering and Science* 1(1): 7–14.

Franssila, Sami. 2010. Introduction to Microfabrication *Introduction to Microfabrication*.

Group, Francis. 2006. *Nanomanufacturing*.

Harb, A., and M. Istanbullu. 2022. “Design and Simulation of a Graphene Based Dual-Gate IonSensitive Field-Effect Transistor (ISFET) Microsensor.” In *BIOMED2022, The 26th Biomedical Science and Technology Symposium*, , 166–73.

Harb, A., & Istanbullu, M. (2023). High Sensitive pH Sensor with Graphene based Dual-Gate ISFET. Journal of NanoScience in Advanced Materials, 2(1), 19–24.

Hassanin, Hany et al. 2019. “Manufacturing Processes for Ceramic and Metal Microcomponents.” 28.

Huang, Ting et al. 2022. “Graphene-Based Ion-Selective Field-Effect Transistor for Sodium Sensing.” *Nanomaterials* 12(15).

Islam, M. J. et. al. 2017. “Study of Characteristics Curves Top-Gated Graphene FET Using SILVACO TCAD.” *Journal of Electronic Design Engineering* 3(3): 1–9.

İstanbullu, Mustafa, and Mutlu Avcı. 2020. *Mikroelektronik Laboratuvar Uygulamaları 2*.

Jung, Su-Ho et al. 2021. “Super-Nernstian PH Sensor Based on Anomalous Charge Transfer Doping of Defect-Engineered Graphene.” *Nano Letters* 21(1): 34–42.

Kajale, Shivam Nitin et al. 2021. “2D Material Based Field Effect Transistors and Nanoelectromechanical Systems for Sensing Applications.” *iScience* 24(12): 103513. https://doi.org/10.1016/j.isci.2021.103513.

Kotsakis, Stathis D. et al. 2021. “Detection of Carbapenemase Producing Enterobacteria Using an Ion Sensitive Field Effect Transistor Sensor.” *Scientific Reports* 11(1): 1–14. https://doi.org/10.1038/s41598-021-91202-6.

Kumar, Sachin, Babankumar, Thakur Ritula, and Manish Kumar. 2015. “Soil PH Sensing Techniques and Technologies- A Review.” *Soil pH Sensing Techniques and Technologies-A Review* 4(5): 4452–56.

Lu, Chih Hung, Tuo Hung Hou, and Tung Ming Pan. 2018. “High-Performance Double-Gate α-InGaZnO ISFET PH Sensor Using a HfO2 Gate Dielectric.” *IEEE Transactions on Electron Devices* 65(1): 237–42.

Ma, Xiaohao et al. 2022. “Recent Advances in Ion-sensitive Field-effect Transistors for Biosensing Applications.” *Electrochemical Science Advances* (September 2021): 1–20.

Mappes, John. 2022. “Development of a Verilog-a Compatible Model for the Fermi Velocity in Graphene Field Effect Transistor Simulations.” *Book*. “Marc Madou.Pdf.”

Mohammadi, Ehsan, and Negin Manavizadeh. 2019. “Performance Evaluation of Innovative Ion-Sensitive Field Effect Diode for PH Sensing.” *IEEE Sensors Journal* 19(4): 1239–44.

Nakata, Shogo, Takayuki Arie, Seiji Akita, and Kuniharu Takei. 2017. “Wearable, Flexible, and Multifunctional Healthcare Device with an ISFET Chemical Sensor for Simultaneous Sweat PH and Skin Temperature Monitoring.” *ACS Sensors* 2(3): 443–48.

Norzin, Mas Syarafina et al. 2018. “PH Sensing Characteristics of Silicon Nitride as Sensing Membrane Based ISFET Sensor for Artificial Kidney.” *IEEE International Conference on Semiconductor Electronics, Proceedings, ICSE* 2018-Augus: 124–27.

Pares-Casanova, Pere M. 2017. “World ’ s Largest Science , Technology & Medicine Open Access Book Publisher Introductory Chapter : Introductory Chapter : Inflammatory Inflammatory Bowel.”

Pullano, Salvatore A. et al. 2019. “Deep Submicron EGFET Based on Transistor Association Technique for Chemical Sensing.” *Sensors (Switzerland)* 19(5): 1–13.

Savadjiev, Gueorgui. 2020. “Design and Fabrication of an Ion Sensitive Field Effect Transistor and Readout Circuit Using a Commercial TSMC 65nm Process.” (May).

Sinha, Soumendu et al. 2021. “Fabrication, Characterization, and Modeling of an Aluminum Oxide-Gate Ion-Sensitive Field-Effect Transistor-Based PH Sensor.” *Journal of Electronic Materials* 50(12): 7085–97.

Tian, Jing, Anestis Katsounaros, Darryl Smith, and Yang Hao. 2015a. “Graphene Field-Effect Transistor Model with Improved Carrier Mobility Analysis.” *IEEE Transactions on Electron Devices* 62(10): 3433–40.

Wang, Hui, and Naiyun Tang. 2021. “A Modified TCAD Simulation Model for A-InGaZnO Based ISFETs on GaAs Substrate for PH Sensing Applications.” *Materials Research Express* 8(9).

Wei, Wei et al. 2020. “Extended Gate Ion-Sensitive Field-Effect Transistors Using Al2O3/Hexagonal Boron Nitride Nanolayers for PH Sensing.” *ACS Applied Nano Materials* 3(1): 403–8.

Werner, Jan et al. 2021. “Characterization of a Fast Response Fiber-Optic PH Sensor and Measurements in a Biological Application.” : 6.

Wu, Chi Chang, and Min Rong Wang. 2021. “Effects of Buffer Concentration on the Sensitivity of Silicon Nanobelt Field-Effect Transistor Sensors.” *Sensors* 21(14).

Wu, Mo, Y. I. Alivov, and Hadis Morkoç. 2008. “High-κ Dielectrics and Advanced Channel Concepts for Si MOSFET.” *Journal of Materials Science: Materials in Electronics* 19(10): 915–51.

Wu, Yung Chen, Shang Jing Wu, and Che Hsin Lin. 2015. “High Performance EGFET-Based PH Sensor Utilizing Low-Cost Industrial-Grade Touch Panel Film as the Gate Structure.” *IEEE Sensors Journal* 15(11): 6279–86.

Yu, Ling-shan et al. 2020. “Crossm Rapid Detection of Azole-Resistant Aspergillus Fumigatus In.” (June): 1–11.

CURRICULUM VITAE

Ahmed W. M. HARB, graduated from Adnan Al-Alamy High School in 2014 and then enrolled to the Biomedical Department at Al-Azhar University-Gaza in the same year. He has graduate with an excellent GPA with a second honor degree in the bachelor level; As a result, I was assigned to work as a Teacher Assistant for two years in the College of Engineering and Information Technology He joined the Biomedical Engineering master's program at Çukurova University in 2021.

APPENDICES

APPENDEX A: TCAD Silvaco ATHENA code

```
go athena
#simflags="-P all"
line x loc=0.0 spacing=0.1
line x loc=0.125 spacing=0.006
line x loc=0.3 spacing=0.006

line y loc=0.0 spacing=0.002
line y loc=0.1 spacing=0.005
line y loc=0.25 spacing=0.05
line y loc=0.4 spacing=0.15

init GaAs orientation=100 c.boron=10e15 space.mul=2 two.d
diffuse time=30 temp=1000 dryo2 press=1.00 hcl=3
structure outfile=ml.str
#tonyplot -st m1.str
#etch oxide thick=0.02

diffuse temp=950 time=100 weto2 hcl=3
structure outfile=m4.str
#tonyplot -st m4.str

diffus time=50 temp=1000 t.rate=4.00 dryo2 press=0.10 hcl=3
diffus time=220 Temp=1200 nitro press=1
diffus time=90 temp=1200 t.rate=-4.444 nitro press=1
structure outfile=m5.str
#tonyplot -st m5.str
etch oxide all
structure outfile=m6.str
#tonyplot -st m6.str

#deposit oxide thick=0.15
diffus time=100 temp=950 dryo2 press=3 hcl=3
structure outfile=m8.str
tonyplot -st m8.str
```

```
deposit polysilicon thick=0.010   c.arsenic=10e15

deposit material=Sapphire thick=0.010

etch material=Sapphire left p1.x=0.22

#GaP

deposit material=germanium thick=0.20 c.boron=1e11

etch material=germanium left p1.x=0.22

deposit aluminum thick=0.05

etch aluminum right p1.x=0.15

#

deposit material=Gold thick=0.015

etch material=Gold left p1.x=0.22


structure outfile=m10.str

#tonyplot -st m10.str

#####################  MIRROR struct mirror right

structure outfile=m17.str

#tonyplot -st m17.str


electrode name=gate x=0.3 y=-0.01

electrode name=source x=0.1

electrode name=drain x=0.5

electrode name=substrate backside

structure outfile=G-ISFET.str

tonyplot -st G-ISFET.str


#extract name="Vt" 1dvt ntype qss=1e10  x.val=0.0 datafile="results23061303.final

extract name="Sheet_R" sheet.res material="Polysilicon" mat.occno=1 x.val=0.3 region.occno=1 semi.poly
datafile="results23061303.final"

extract name="JunctionDepth" xj material="Polysilicon" mat.occno=1 y.val=-0.16 datafile="results23061303.final"
junc.occno=1

#extract name="Qick" 1dvt ntype x.val=0.3

#extract name="Scons" surf.conc impurity="Net Doping" material="Polysilicon" mat.occno=1 x.val=0.3
datafile="res230607.final"

#extract name="vt" (xintercept(maxslope(curve(abs(v."gate"),abs(i."drain")))) - abs(ave(v."drain"))/2.0)


#extract name="Conduction Band" curve(depth, impurity="Conduction Band Energy" material="All" x.val=0.3)
outfile="res23060701.final" #

#output j.electron j.hole j.conduc j.total ex.field ey.field flowlines e.mobility h.mobility e.temp h.temp con.band qfn
j.disp photogen impact

#save outf=Charac230607
```

```
#extract init infile="GaNRTD_init.str"

#extract name="Conduction Band" curve(depth, impurity="Conduction Band Energy" material="All" x.val=0.005)
outfile="GaNRTD_init.dat"

#extract name="Valence Band" curve(depth, impurity="Valence Band Energy" material="All" x.val=0.005)
outfile="GaNRTD_init_VB.dat"

#extract name="Electric Field" curve(depth, impurity="E Field" material="All" x.val=0.005)
outfile="GaNRTD_init_EF.dat"

#////////////////////////////////// ATLAS //////////////////////////////////////

go atlas

contact name=gate aluminum

contact name=drain aluminum

contact name=substrate aluminum

material material= germanium  user.group=semiconductor user.default=silicon eg300=1 nc300=4e27 nv300=4e21
permittivity=80 affinity=3.9

#0.186

material polysilicon  user.group=semiconductor user.default=silicon eg300=0.1 nc300=377e15 nv300=377e15
permittivity=80 MUN=300 MUP=30

##########Id/Vg ##########

solve vdrain=2.2 vgate=-1.1 outfile=solve1

#solve vdrain=1 vsubstrate=0 outfile=solve2

#solve vdrain=1.5 vsubstrate=0 outfile=solve3


load infile=solve1

log outfile=ph10.log

solve name=substrate vsubstrate=0 vfinal=10 vstep=0.4

##

#load infile=solve2

#log outfile=Vds1.log

#solve name=gate vgate=-1 vfinal=3 vstep=0.3

##

#load infile=solve3

#log outfile=Vds1.5.log

#solve name=gate vgate=-1 vfinal=3 vstep=0.3


#tonyplot  -overlay ChThick1nm.log ChThick5nm.log ChThick15nm.log ChThick20nm.log

#tonyplot -overlay Vds0.5.log Vds1.log  Vds1.5.log

#tonyplot -overlay Vgs0.log Vgs1.log  Vgs2.log Vgs3.log

tonyplot   -overlay  ph4.log ph7.log ph10.log

quit
```

APPENDEX B: Verilog-A code for Gr_ISFET model

```
`include "disciplines.vams"
`include "constants.vams"
`include "compact.vams"
`define FWD 1
`define REV -1
// AB 040902
`define NOT_GIVEN -1.0e21
`define DEFAULT_TNOM 25
module ekv_va(d,g,s,b);
  // %%DEVICE_CLASS=MOS(NMOS:TYPE=1,PMOS:TYPE=-1)%%
  //  Node definitions
  inout          d,g,s,b;        // external nodes
  electrical     d,g,s,b;        // external nodes
  //      Branch definitions
  branch (d,s)    ds;
  branch (d,b)    db;
  branch (s,b)    sb;
  branch (g,b)    gb;
  // * Local variables
  real tmp1, tmp2, tmp3; // temporary variables
  real VGprime, GAMMAprime;// short and narrow channel effect
  real VP, VPprime;    // pinch-off voltage
  real if_, ir, irprime;   // normalized currents
  real VDSS, VDSSprime;// saturation voltage
  real deltaL, Leq;    // channel length reduction
  real beta;           // transconductance factor
  real n;              // slope factor
  real Ispec;          // specific current
  real Vt;             // k*T/q
  real gm, gms, gmbs, gds;
  real isub, Isub;
  real inv_Vt, Vt_01, Vt_2, Vt_4, Vt_Vt, Vt_Vt_2, Vt_Vt_16;
  real eps_COX, eps_COX_W, eps_COX_L;
  real Lc, Lc_LAMBDA, IBN_2, T0, T1, eta_qi;
  real inv_UCRIT, Lc_UCRIT, Lc_IBB, IBA_IBB;
```

```
integer Mode;
real WETA_W, LETA_L;
real E0_Q_1, AWL;
real T, KP_Weff;
real Eg, refEg, deltaT, ratioT, Tnom;
real VTO_T, VTO_S, KP_T, UCRIT_T, IBB_T, PHI_T, GAMMA_S;
real sqrt_Lprime_Lmin;
real GAMMAstar, sqrt_GAMMAstar;
real big_sqrt_VP;
real big_sqrt_VP0, VP0;
real PHI_VD, PHI_VS;
real sqrt_PHI;
real sqrt_PHI_VP, sqrt_PHI_VD, sqrt_PHI_VS;
real sqrt_PHI_VD_Vt, sqrt_PHI_VS_Vt;
real Vds, deltaV_2, Vip;
real VDSS_sqrt, sqrt_VDSS_deltaV, sqrt_Vds_VDSS_deltaV;
real VDSSprime_sqrt, sqrt_VDSSprime_deltaV, sqrt_Vds_VDSSprime_deltaV;
real if_ir;
real sqrt_if, sqrt_ir, sqrt_irprime;
real dif_dv, dir_dv, dirprime_dv;
//  Charge related variables
real sif, sir, sif2, sir2, sif3, sir3;
real sif_sir_2;
real qi, qb;
real QD, QS, QI, QB, QG;
real VP_PHI_eps, sqrt_PHI_VP_2, WLCox;
real n_Vt_COX, n_1, n_1_n;
//  Variables used for derivatives computation
real dVP_dVD, dVP_dVG, dVP_dVS;
real dif_dVD, dif_dVS, dif_dVG;
real dir_dVD, dir_dVS, dir_dVG;
real dVDSS_dVD, dVDSS_dVG, dVDSS_dVS;
real ddeltaV_dVD, ddeltaV_dVG, ddeltaV_dVS;
real dVip_dVD, dVip_dVG, dVip_dVS;
real dVDSSprime_dVD, dVDSSprime_dVG, dVDSSprime_dVS;
real dirprime_dVD, dirprime_dVG, dirprime_dVS;
real dLeq_dVD, dLeq_dVG, dLeq_dVS;
real dbeta_dVD, dbeta_dVG, dbeta_dVS;
```

```
    real VGstar, sqrt_VGstar;
    real VG, VD, VS;
    real Von, Vdsat, Id, Ibd;
    real Gn;
    real GAMMA_sqrt_PHI, Lmin, Lprime, T0_GAMMA_1, THETA_VP_1, Vc;
    real Vdsprime, Vt_Vc, dGAMMAprime_dVD, dGAMMAprime_dVG, dGAMMAprime_dVS;
    real dVPprime_dVD, dVPprime_dVG, dVPprime_dVS, ddeltaL_dVD, ddeltaL_dVG;
    real ddeltaL_dVS, dn_dVD, dn_dVG, dn_dVS;
    real log_Vc_Vt, sqrt_PHI_VP0, sqrt_VP_Vt;
    real Lc_IBB_Vib, Vib, dIsub_factor, exp_ib;
    real inv_Vib, sqrt_PHI_VP2_2;
    real V0, deltaVFB, vL;
    real dQI_dVD, dQI_dVS, dQI_dVG;
    real dQB_dVD, dQB_dVS, dQB_dVG;
    real Leff, Weff;
    real RSeff, RDeff;
    real yk, z0, zk;
    real EPSOX, epssil;
    real ddt_QD, ddt_QS;
    //DIODES realted variables [AB: 040902]
    real as_i, ad_i, ps_i, pd_i, v_di_b, v_si_b;
    real temp_arg, tmp0;
    real js_t, jsw_t, jswg_t;
    real pb_t, pbsw_t, pbswg_t;
    real cj_t, cjsw_t, cjswg_t;
    real njts_t, njtssw_t, njtsswg_t;
    real is_d, arg_d, is_s, arg_s;
    real f_breakdown_d, f_breakdown_s, idb_tun, isb_tun;
    real csb_d, cssw_d, csswg_d;
    real csb_s, cssw_s, csswg_s;
    real qjd, qjs;

    // parameter definitions
    parameter integer TYPE = 1 from [-1:1] exclude 0; // NMOS=1, PMOS=-1
    parameter integer Noise = 1 from [0:1];     // Set to zero to prevent noise calculation
    parameter real Trise = 0.0 from [-inf:inf]; // Difference sim. temp and device temp [C deg]
//  parameter real Temp = -`NOT_GIVEN from [`P_CELSIUS0:inf];  // Device temp [C]
//AB:  the parameter name Temp is not working for no obvious reason; changed to TEMP
```

```
parameter real TEMP = -`NOT_GIVEN from [`P_CELSIUS0:inf];  // Device temp [C]
parameter real TNOM = -`NOT_GIVEN; // Temperature [C]
parameter real L = 10E-6 from [0.0:inf]; // Channel length [m]
parameter real W = 10E-6 from [0.0:inf]; // Channel width [m]
parameter real M = 1.0 from [0.0:inf]; // Parallel multiple device number
parameter real NS = 1.0 from [0.0:inf]; // Series multiple device number
parameter real AS = 0.0 from [0.0:inf]; // Source area       //AB: 040902
parameter real AD = 0.0 from [0.0:inf]; // Drain area        //AB: 040902
parameter real PS = 0.0 from [0.0:inf]; // Source perimeter             //AB: 040902
parameter real PD = 0.0 from [0.0:inf]; // Drain perimeter              //AB: 040902
// *** Process related parameters
parameter real COX = 2.0E-3 from [0.0:inf]; // Gate oxide capacitance per unit area [F]
parameter real XJ = 300E-9 from [0.0:inf]; // Junction depth [m]
//*** Threshold voltage/substrate effect parameters (long-channel)
parameter real VTO = 0.5 from [-inf:inf]; // Long-channel threshold voltage [V]
parameter real TCV = 1.0e-3; // Threshold voltage temperature coefficient [V/K]
parameter real GAMMA = 0.7 from [0.0:inf]; // Body effect parameter
parameter real PHI = 0.5 from [0.2:inf]; // Bulk Fermi potential [V]
//*** Mobility parameters (long-channel) ***
parameter real KP = 150E-6 from [0.0:inf]; // Transconductance parameter [A/V/V]
parameter real BEX = -1.5; // Mobility temperature exponent
parameter real THETA = 0.0 from [0.0:inf]; // Mobility reduction coefficient [1/V]
parameter real E0 = 1.0E8; // Mobility reduction coefficient [V/m]
//*** Velocity sat./channel length mod. parameters (short-channel)
parameter real UCRIT = 2.0E6 from [0.0:inf]; // Longitudinal critical field [V/m]
parameter real UCEX = 0.8; // Longitudinal critical field temperature exponent
parameter real LAMBDA = 0.8 from [0.0:inf]; // Depletion length coefficient (channel length modulation)
//*** Process related parameters
parameter real DL = -0.01E-6; // Channel width correction [m]
parameter real DW = -0.01E-6; // Channel length correction [m]
//*** Threshold voltage/substrate effect parameter (narrow-channel)
parameter real WETA = 0.2 from [0.0:inf]; // Narrow-channel effect coefficient
//*** Threshold voltage/substrate effect parameters (short-channel)
parameter real LETA = 0.3 from [0.0:inf]; // Short-channel effect coefficient
parameter real Q0 = 230E-6 from [0.0:inf]; // Reverse short channel effect peak charge density
parameter real LK = 0.4E-6 from [0.0:inf]; // Reverse short channel effect characteristic length [m]
//*** Substrate current parameters
parameter real IBA = 5.0E8 from [0.0:inf]; // First impact ionization coefficient [1/m]
```

```
parameter real IBB = 4.0E8 from [0.0:inf]; // Second impact ionization coefficient [V/m]
parameter real IBBT = 9.0e-4; // Temperature coefficient for IBB [1/K]
parameter real IBN = 1.0 from [0.0:inf]; // Saturation voltage factor for impact ionization
//*** Series resistance parameters
parameter real RSH = 0.0 from [0.0:inf]; // Sheet resistance [Ohms]
parameter real HDIF = 0.5E-6 from [0.0:inf]; // Sheet resistance multipler
//*** for MC analysis fk 25/05/97
parameter real AVTO = 1E-6 from [0.0:inf]; // Area related threshold voltage mismatch parameter [Vm]
parameter real AKP = 1E-6 from [0.0:inf]; // Area related gain mismatch parameter [m]
parameter real AGAMMA = 1E-6 from [0.0:inf]; // Area related body effect mismatch parameter [sqr(V) m]
parameter real AF = 1.0 from (0:inf); // Flicker noise exponent
parameter real KF = 0.0 from [0:inf); // Flicker noise coefficient
//*** JUNCTION DRAIN-BULK AND SOURCE-BULK AREA, CURRENT, CAPACITANCE [AB:040902]
parameter real xd_n          = 1.0          from [0.0:inf);
parameter real xd_js         = 1.0E-09      from [0.0:inf);
parameter real xd_jsw        = 1.0E-12      from [0.0:inf);
parameter real xd_jswg       = 1.0E-12      from [0.0:inf);
parameter real xd_mj         = 0.900        from [0.0:1.0];
parameter real xd_mjsw       = 0.700        from [0.0:1.0];
parameter real xd_mjswg      = 0.700        from [0.0:1.0];
parameter real xd_pb         = 0.800        from (0.0:inf);
parameter real xd_pbsw       = 0.600        from (0.0:inf);
parameter real xd_pbswg      = 0.600        from (0.0:inf);
parameter real xd_cj         = 1.0E-09      from [0.0:inf);
parameter real xd_cjsw       = 1.0E-12      from [0.0:inf);
parameter real xd_cjswg      = 1.0E-12      from [0.0:inf);
parameter real xd_gmin       = 0.0          from [0.0:inf);
parameter real xd_xjbv       = 0.0          from [0.0:inf);
parameter real xd_bv         = 10.0         from [0.0:inf);
parameter real xd_njts       = 1.0          from [0.0:inf);
parameter real xd_njtssw     = 1.0          from [0.0:inf);
parameter real xd_njtsswg    = 1.0          from [0.0:inf);
parameter real xd_vts        = 0.0          from [0.0:inf);
parameter real xd_vtssw      = 0.0          from [0.0:inf);
parameter real xd_vtsswg     = 0.0          from [0.0:inf);
parameter real tp_xti        = 3.0          from (-inf:inf);
parameter real tp_cj         = 0.0          from (-inf:inf);
parameter real tp_cjsw       = 0.0          from (-inf:inf);
```

```
parameter real tp_cjswg      = 0.0          from (-inf:inf);
parameter real tp_pb         = 0.0          from (-inf:inf);
parameter real tp_pbsw       = 0.0          from (-inf:inf);
parameter real tp_pbswg      = 0.0          from (-inf:inf);
parameter real tp_njts       = 0.0          from [0.0:inf);
parameter real tp_njtssw     = 0.0          from [0.0:inf);
parameter real tp_njtsswg    = 0.0          from [0.0:inf);
analog begin
   // Set constant
   EPSOX  = 3.9 * `P_EPS0;
   epssil = 11.7 * `P_EPS0;
   Ibd = 0.0;
   // The following are necessary to prevent memory states being reserved:
   THETA_VP_1 = 0.0;
   VPprime = 0.0;
   sqrt_VP_Vt = 0.0;
   // Geometry, voltage and temperature independent model variables
   eps_COX = epssil/COX;
   Lc  = sqrt(eps_COX*XJ);
   Lc_LAMBDA  = Lc * LAMBDA;
   eps_COX_W = 3.0 * eps_COX * WETA;
   eps_COX_L = eps_COX * LETA;
   IBN_2 = IBN + IBN;
   T0 = COX / (epssil*E0);
   V0 = (Q0+Q0) / COX;
   eta_qi = TYPE > 0 ? 0.5 : 0.3333333333333;
   /* Model working variables, geometry and voltage independent,
    * which need to be updated after temperature change
    * EKV model internal variables depending on temperature.
    */
   /* If Temp is explicitly specified, use that value
      otherwise use Tckt+Trise */
   if (TEMP == -`NOT_GIVEN)       //AB: 040902 Temp -> TEMP
      T = $temperature + Trise;
   else
      T = TEMP + `P_CELSIUS0;     //AB: 040902 Temp -> TEMP
   if (TNOM == -`NOT_GIVEN)
      Tnom = `DEFAULT_TNOM + `P_CELSIUS0;
```

```
else
   Tnom = TNOM + `P_CELSIUS0;
Vt = $vt(T);
Vt_01 = 0.1 * Vt;
inv_Vt = 1.0 / Vt;
Vt_2 = Vt + Vt;
Vt_4 = Vt_2 + Vt_2;
Vt_Vt = Vt * Vt;
Vt_Vt_2 = Vt_Vt + Vt_Vt;
Vt_Vt_16 = 16.0 * Vt_Vt;

Eg = 1.16 - 7.02e-4 * T * T / (T + 1108.0);
refEg = 1.16 - (7.02e-4*Tnom*Tnom) / (Tnom + 1108.0);
deltaT = T - Tnom;
ratioT = T / Tnom;
VTO_T = VTO - TCV * deltaT;
KP_T = KP * pow(ratioT, BEX);
UCRIT_T = UCRIT * pow(ratioT, UCEX);
IBB_T = IBB * (1.0 + IBBT * deltaT);
PHI_T = PHI * ratioT - 3.0 * Vt * ln(ratioT) - refEg * ratioT + Eg;
//  !!  mb  99/07/30  prevents PHI from becoming smaller than 0.2
tmp1 = 0.2;
tmp2 = PHI_T - tmp1;
PHI_T = 0.5*(tmp2 + sqrt(tmp2*tmp2 + Vt*Vt)) + tmp1;
sqrt_PHI = sqrt(PHI_T);
inv_UCRIT = 1.0/UCRIT_T;
Lc_UCRIT  = Lc * UCRIT_T;
Lc_IBB  = Lc * IBB_T;
IBA_IBB = IBA / IBB_T;
/* VTO, KP and GAMMA with variation for MC analysis if required.
 * The default value for model parameters AVTO, AKP and AGAMMA
 * is set to 1e-6 to allow meaningful sensitivity analysis. Only
 * the deviation from this value has to be taken into account
 */
// wg: for userc.c and verilog implementations
Leff = L + DL;
// wg: for userc.c and verilog implementations
Weff = W + DW;
```

```
    Vc = UCRIT_T*Leff;   //  NOTE: use L if necessary
    log_Vc_Vt = Vt*(ln(0.5*Vc*inv_Vt)-0.6);   //    mb  98/02/05  (r1)
    // de-normalization
    AWL = 1.0/sqrt(Weff*Leff);
    if (TYPE > 0)
       VTO_S  = ((AVTO != 1e-6) ? AWL*(AVTO - 1e-6) + VTO_T : VTO_T);
    else
       VTO_S  = ((AVTO != 1e-6) ? AWL*(1e-6 - AVTO) - VTO_T: -VTO_T);
    KP_Weff = Weff * ((AKP != 1e-6) ? KP_T*(1 + (AKP - 1e-6)*AWL) : KP_T);
    GAMMA_S = ((AGAMMA !=1e-6) ? GAMMA + (AGAMMA - 1e-6)*AWL : GAMMA);
    GAMMA_sqrt_PHI = GAMMA_S*sqrt_PHI;

endmodule
```

APPENDEX C: Verilog-A code for Electrolyte model

```
`include "constants.vams"
`include "disciplines.vams"

//define relative permittivity of water
`define RP_EPSw 80
//conversion constant from moles/liter to #/m^3
`define N_AVG 6e26

module pH_robust_model_1_0_1(fgate,interface,pHnode);

 input pHnode;
 output fgate,interface;              // fgate is connected to the reference electrode, interface is in contact with the surface
 electrical fgate,interface,pHnode;
//Convention for Ka, Kb: Ka=[A-OH][Hs+]/([AOH2+], Kb=[AO-][Hs+]/[AOH]
//NOH_SI denotes the charge density of the surface groups: NOH_SI=[AOH]+[AO-]+[AOH2+]
// pH=-log10[H+], pKa=-log10[Ka], pKb=-log10[Kb]
//Parameters characterizing electrolyte and electrolyte-oxide interface
parameter real version        =   1.00;                    // pHsensor surface potential model version = 1.0.1
parameter real sternmod       =   1      from [0:1];       // Parameter to turn on/off the stern model. 0 means that the
model is off.
parameter real pKa            =   -2.0    from (-inf:inf);  // pKa of the acidic [A-OH2+] surface group
parameter real pKb            =   6.0     from (-inf:inf);  // pKb of the basic [A-OH] surface group
parameter real i0             =   0.1     from [0.0:inf];   // ionic concentration in moles/liter
parameter real Cstern         =   0.2     from (0.0:inf];   // Stern capacitance in F/m^2
parameter real NOH            =   5e14    from (0.0:inf);   // Number density of surface OH groups in cm^-2

real pH;
real ew;
real n0;
real pzc, deltapK;
real NOH_SI;
real c, deltapH;

//parameters to be used for calculation
```

```
real Q0dl, Q0, Qratio, dpH;
real vfi, tanhvfi, norm_QOH;

analog begin
    pzc         =     (pKa+pKb)/2.0;
//pHpzc is the point of zero charge i.e. pH at which the surface charge is zero assuming that surface potential is zero
    deltapK     =     pKb-pKa;
    pH          =     V(pHnode);
    deltapH     =     pH-pzc;
    c           =     limexp(`M_LN10*deltapK/2.0);
    Q0          =     2*`P_Q*NOH_SI;
    dpH         =     `M_LN10*deltapH;
    NOH_SI      =     NOH * 1e4;                    // conversion from cm^-2 to m^-2
    n0          =     `N_AVG*i0;                    // conversion to #/m^3  (ionic concentration)
    ew          =     `RP_EPSw*`P_EPS0;             // permittivity of the electrolyte, in units of F/m
    Q0dl        =     sqrt(8.0 * ew * $vt * `P_Q * n0);     // prefactor for the double layer charge (in units of columb/cm^2)
    Qratio      =     Q0/Q0dl;
    vfi         =     V(interface,fgate);
    tanhvfi     =     tanh(vfi/$vt+dpH);
    norm_QOH    =     tanhvfi/ (2.0+c*sqrt(1.0-tanhvfi*tanhvfi));

  if(sternmod == 0) begin
      V(interface,fgate) <+ 2*$vt*asinh(-Qratio*norm_QOH);     // Refer Section 3.2.1 of the manual
    end
  else begin
      V(interface,fgate) <+ 2*$vt*asinh(-Qratio*norm_QOH)-Q0/Cstern*norm_QOH;    // Refer Section 3.2.2 of the manual
    end
  end

endmodule
```